Scientia Iranica A (2017) 24(5), 2346–2368

Sharif University of Technology
Scientia Iranica
Transactions A: Civil Engineering
www.scientiairanica.com

Innovative analytical solutions to 1, 2, and 3D water infiltration into unsaturated soils for initial-boundary value problems

H.R. Zarif Sanayei*, G.R. Rakhshandehroo and N. Talebbeydokhti

Department of Civil and Environmental Engineering, Shiraz University, Shiraz, Iran.

Received 10 January 2016; received in revised form 27 April 2016; accepted 5 July 2016

KEYWORDS
Richards' equation;
Analytical solution;
Infiltration;
Unsaturated soil;
Initial-boundary value problems.

Abstract. Fluid infiltration into unsaturated soil is of vital significance from many perspectives. Mathematically, such transient infiltrations are described by Richards' equation: a nonlinear parabolic Partial Differential Equation (PDE) with limited analytical solutions in the literature. The current study uses separation of variables and Fourier series expansion techniques and presents new analytical solutions to the equation in one, two, and three dimensions subject to various boundary and initial conditions. Solutions for 1D horizontal and vertical water infiltration are derived and compared to numerical finite-difference method solutions, whereby both solutions are shown to coincide well with one another. Solutions to 2 and 3D vertical water infiltration are derived for constant, no-flow, and sinusoidal boundary and initial conditions. The presented analytical solutions are such that both steady and unsteady solutions may be obtained from a single closed form solution. The solutions may be utilized to test numerical models that use different computational techniques.

1. Introduction

Fluid infiltration into unsaturated soil is of vital significance from many perspectives. Hydrogeologists, environmentalists, and water resource planners view water and pollutant infiltration into unsaturated zone from their own standpoints. A phreatic aquifer is replenished from above by water from various sources: precipitation, irrigation, artificial recharge, etc. In all cases, water moves downward, from ground surface to the water table, through the unsaturated zone. The understanding of and, consequently, the ability to calculate and predict the movement of water in the unsaturated zone is essential when we wish to determine the replenishment of a phreatic aquifer [1].

Transient fluid flow through unsaturated soil is usually described by Richards' equation derived by combining Darcy's law and conservation of mass. The equation is a nonlinear parabolic Partial Differential Equation (PDE) for which many numerical and limited analytical solutions exist.

In the last two decades, many numerical techniques have been proposed to investigate water flow infiltration through unsaturated soils. These techniques include Finite-Difference Method (FDM), Finite-Element Method (FEM), Finite Volume Method (FVM), hp-FEM and time splitting method [2-11]. Analytical solutions, on the other hand, are mainly offered for one-dimensional flow of water through the soil and for restrictive boundary and initial conditions. Exact analytical solutions are desirable because they

*. *Corresponding author.*
E-mail address: hzarif63@gmail.com (H.R. Zarif Sanayei)

doi: 10.24200/sci.2017.4161

give a better insight compared to a discrete numerical solution. As such, analytical solutions may be used as benchmark or reference results to test and verify numerical algorithms and codes. Though useful, analytical solutions to transient water infiltration into unsaturated soil samples for various boundary and initial conditions are still lacking.

Parlange et al. [12] presented a general approximation for a solution to 1D Richards' equation. Mollerup [13] used Philip equation, and showed that the power series solution may be applied to variable-head ponded infiltration, when the ponding depth is described as a power series. Menziani et al. [14] presented solutions to the linearized one-dimensional Richards' equation for discrete arbitrary initial and boundary conditions. The result was soil water content at any required time and depth in a domain of semi-infinite unsaturated porous medium. Tracy [15] developed clean two- and three-dimensional analytical solutions to Richards' equation for testing numerical solvers.

In addition, Tracy [16] obtained three-dimensional analytical solutions to Richards' equation when a box-shaped soil sample with piecewise constant head boundary conditions on the top is utilized.

Wang et al. [17] developed an algebraic solution to one-dimensional water infiltration and redistribution without evaporation. They established a relationship between Green-Ampt model and the algebraic solution to analyze physical features of the soil parameters. Ghotbi et al. [18] applied Homotopy Analysis Method (HAM) to solve the equation analytically, and showed that the method is superior to traditional perturbation techniques in the sense that it is not dependent on the assumption of a small parameter as the initial step. Nasseri et al. [19] presented three major cases for the governing PDE solved by Traveling Wave Solution (TWS) method using general and modified forms of *tanh* functions. They used TWS as an initial value problem and considered the typical forms of diffusivity and conductivity functions proposed by Brooks and Corey [20]. Huang and Wu [21] developed analytical solutions to 1D horizontal and vertical water infiltration into saturated-unsaturated soils. They considered variations of influx over time. Asgari et al. [22] applied exp-function method to 1D Richards' equation to evaluate its effectiveness and reliability and to reach a more generalized solution to the problem. They used Brooks and Corey [20] model for soil properties. Basha [23] developed approximate solutions to Richards' equation for rational forms of the soil hydraulic conductivity and moisture retention functions by a perturbation expansion method.

A number of researchers investigated analytical solutions to the 1D Richards' equation by Variational Iteration Method (VIM) [24-26] and Adomian Decomposition Method (ADM) [27-31]. They used ADM and VIM in an initial value problem for the equation; however, the series solution obtained by ADM and VIM often did not satisfy the PDE. A number of researchers studied analytical solutions to Richards' equation in infinite and semi-infinite domains by TWS, Green function, and exponential time integration methods [32-35].

The current study presents new analytical solutions to Richards' equation in one, two, and three dimensions subject to various boundary and initial conditions. First, 1D horizontal and vertical water infiltration solutions are derived, and then results are compared to a numerical finite-difference method solution. Finally, solutions to 2 and 3D vertical water infiltrations are derived for constant, no-flow, and sinusoidal boundary and initial conditions. Solutions are sought in a form that contains both steady and unsteady terms in a single closed form solution. The solutions may be utilized to test numerical models that use different computational techniques.

2. Governing equation

The movement of water flow in unsaturated soil is described by Richards' equation. This equation is developed by the combination of continuity and Darcy's law as a momentum equation. This equation is expressed in different forms. The 3D θ-based form of the equation is [36]:

$$\frac{\partial\theta}{\partial t} = \frac{\partial}{\partial x}\left(D_x(\theta)\frac{\partial\theta}{\partial x}\right) + \frac{\partial}{\partial y}\left(D_y(\theta)\frac{\partial\theta}{\partial y}\right) + \frac{\partial}{\partial z}\left(D_z(\theta)\frac{\partial\theta}{\partial z} + K_z(\theta)\right), \quad (1)$$

where $\theta\left(\frac{L^3}{L^3}\right)$ is the volumetric water content, and $D(\theta) = K(\theta)\frac{\partial h}{\partial\theta}$ is soil water diffusivity for isotropic media; $h(L)$ is the soil water pressure head (tension head in unsaturated zone), $K\left(\frac{L}{T}\right)$ is the hydraulic conductivity, $t(T)$ is the time, and $Z(L)$ is the vertical space coordinate (upward positive). Water diffusivity, hydraulic conductivity, and water content are functions of soil water pressure head. Various empirical relationships have been used to relate K and θ to h [20,37-39]. Basha [33] described K and θ in terms of h by the exponential expression:

$$\frac{\theta-\theta_r}{\theta_s-\theta_r} = S = \exp(\alpha h), \quad (2)$$

$$K(\theta) = K_s\frac{\theta-\theta_r}{\theta_s-\theta_r} = K_s S = K_s\exp(\alpha h), \quad (3)$$

where θ_r is the residual water content, θ_s is the saturated water content, $K_s\left(\frac{L}{T}\right)$ is the saturated hydraulic

conductivity, and $\alpha\left(\frac{1}{L}\right)$ is the pore-sized distributions index. Substituting Eqs. (2) and (3) into $D(\theta)$ gives:

$$D(\theta) = K(\theta)\frac{\partial h}{\partial \theta} = \frac{K_s}{\alpha(\theta_s - \theta_r)}. \tag{4}$$

Replacing Eqs. (2), (3), and (4) into Eq. (1) provides a linear form of Richards' equation:

$$\frac{\partial \theta}{\partial t} = D\frac{\partial^2 \theta}{\partial x^2} + D\frac{\partial^2 \theta}{\partial y^2} + D\frac{\partial^2 \theta}{\partial z^2} + f\frac{\partial \theta}{\partial z}, \tag{5}$$

where D and f are:

$$D = \frac{K_s}{\alpha(\theta_s - \theta_r)}, \qquad f = \frac{K_s}{(\theta_s - \theta_r)}. \tag{6}$$

In the present work, new analytical solutions are derived for Eq. (5) in one, two, and three dimensions subject to various boundary and initial conditions.

3. Analytical solution for 1D horizontal water infiltration

Richards' equation for 1D horizontal flow (x direction) with constant θ_L at the upstream boundary would be:

$$\frac{\partial \theta}{\partial t} = D\frac{\partial^2 \theta}{\partial x^2}, \quad 0 \le x \le L, \qquad t > 0, \tag{7}$$

$$\theta(0,t) = \theta_L, \quad \theta(L,t) = \theta_r,$$

$$\theta(x,0) = \theta_r, \quad \theta_L > \theta_r.$$

The boundary and initial value problem is shown schematically in Figure 1.

A new analytical solution is sought whereby both steady and unsteady solutions may be obtained from a single equation. Such a solution may be expressed as a combination of a steady (W) and an unsteady (V) term:

$$\theta(x,t) = V(x,t) + W(x). \tag{8}$$

Substituting Eq. (8) into Eq. (7) and using separation of variables for $\theta(x,t)$ yields:

$$\theta(x,t) = \sum_{n=1}^{\infty} \frac{2}{n\pi}(\theta_r - \theta_L)\sin\left(\frac{n\pi}{L}x\right) e^{-\left(\frac{n\pi}{L}\right)^2 Dt} + \frac{\theta_r - \theta_L}{L}x + \theta_L. \tag{9}$$

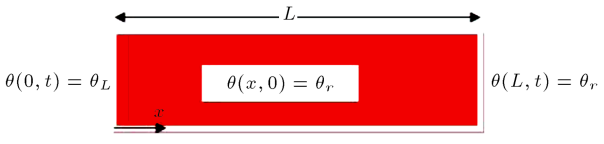

Figure 1. Schematic view of 1D horizontal infiltration problem (x direction).

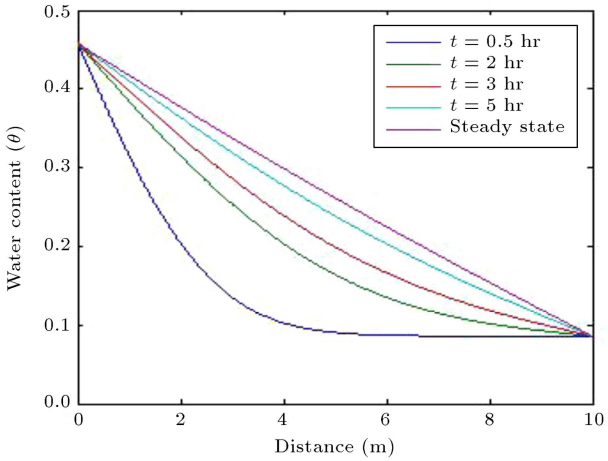

Figure 2. Water content distribution for the analytical solution (Eq. (9)) at $t = 0.5, 2, 3, 5$ hrs and the steady state.

Obviously, Eq. (9) satisfies Eq. (7) and the boundary and initial conditions therein. The first term in Eq. (9), the unsteady term, consists of an exponential expression (with a negative power) in an infinite series. At early times, both V and W contribute to spatiotemporal water content distribution. However, at later times (as $t \to \infty$), V vanishes quickly, and $W(x)$, the steady state term, would be the solution. A plot of Eq. (9) is shown in Figure 2 for the following soil parameters:

$$\theta_L = 0.458, \quad \theta_r = 0.086,$$

$$D = 4\frac{\text{m}^2}{\text{hr}}, \quad L = 10 \text{ m}.$$

As shown, water content profile reflects the unsteady advancing front, which eventually ends up in a linear steady state. Figure 3(a) and (b) show comparisons of a Finite-Difference Method (FDM) solution (to Eq. (7)) by implicit scheme, with the analytical solution for $t = 0.5$ hr and $t = 3$ hr, respectively. The FDM solution was obtained for $\Delta t = 6$ min and $\Delta x = 0.2$ m. As shown, both solutions coincide well with one another.

4. Analytical solution for 1D vertical water infiltration

Richards' equation for 1D vertical flow (z direction) with constant θ_0 at the top boundary would be:

$$\frac{\partial \theta}{\partial t} = D\frac{\partial^2 \theta}{\partial z^2} + f\frac{\partial \theta}{\partial z} \tag{10}$$

$$\theta(0,t) = \theta_r, \quad \theta(L,t) = \theta_0, \quad \theta(z,0) = \theta_r.$$

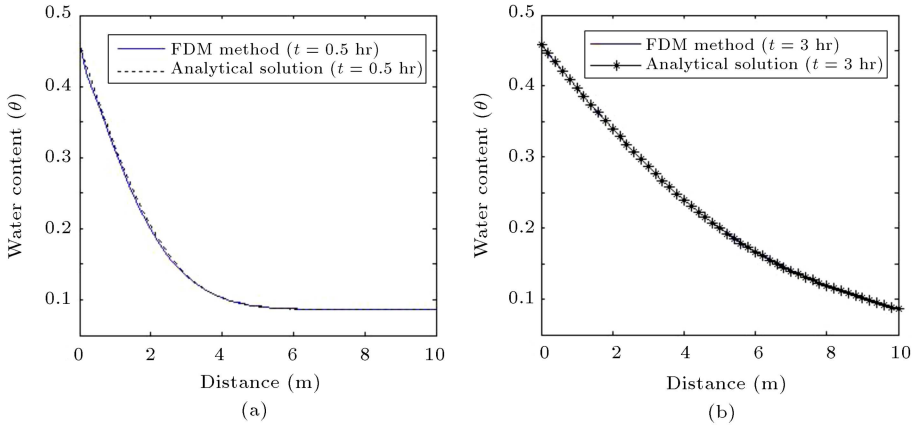

Figure 3. Comparison of water content profiles for the analytical solution (Eq. (9)) and a Finite-Difference Method (FDM): (a) 0.5 hr and (b) 3 hr.

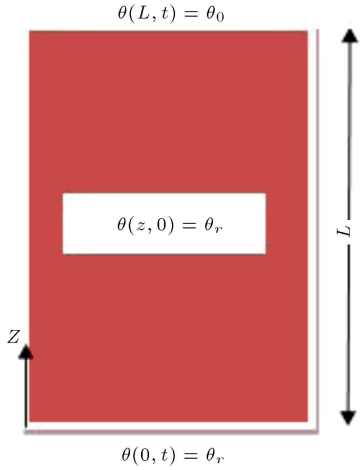

Figure 4. Schematic view of 1D vertical infiltration problem (z direction).

The boundary and initial value problem is shown schematically in Figure 4.

Again, an analytical solution is sought whereby both steady and unsteady solutions may be obtained from a single closed form solution. The general form of the equation is expressed again as a combination of a steady (W) and an unsteady (V) term:

$$\theta(z,t) = V(z,t) + W(z). \tag{11}$$

Substituting Eq. (11) into Eq. (10) and using separation of variables for $\theta(z,t)$ yields:

$$\theta(z,t) = e^{-\frac{f}{2D}z - \frac{f^2}{4D}t} \sum_{n=1}^{\infty} A_n^* \sin\left(\frac{n\pi}{L}z\right) e^{-\left(\frac{n\pi}{L}\right)^2 Dt} + Qe^{-\frac{f}{D}z} + P, \tag{12}$$

where A_n^*, P, and Q are:

$$A_n^* = \frac{2}{L}\int_0^L \left((\theta_r - P)e^{\frac{f}{2D}z} - Qe^{-\frac{f}{2D}z}\right)\sin\left(\frac{n\pi}{L}z\right)dz$$

$$= \frac{2}{L}\left[(\theta_r - P)\frac{-e^{\frac{f}{2D}L}\left(\frac{n\pi}{L}\right)(-1)^n + \left(\frac{n\pi}{L}\right)}{\left(\frac{f}{2D}\right)^2 + \left(\frac{n\pi}{L}\right)^2}\right.$$

$$\left. - Q\frac{-e^{\frac{-f}{2D}L}\left(\frac{n\pi}{L}\right)(-1)^n + \left(\frac{n\pi}{L}\right)}{\left(\frac{f}{2D}\right)^2 + \left(\frac{n\pi}{L}\right)^2}\right], \tag{13}$$

$$P = \frac{\theta_r e^{-\frac{f}{D}L} - \theta_0}{-1 + e^{-\frac{f}{D}L}},$$

$$Q = \frac{(\theta_0 - \theta_r)}{-1 + e^{-\frac{f}{D}L}}.$$

Obviously, Eq. (12) satisfies Eq. (10) and the boundary and initial conditions therein. The first term in Eq. (12), the unsteady term, consists of two exponential expressions in t and z (with negative powers) in and out of an infinite series. The steady term, W, has also an exponential expression in z. At early times, both V and W contribute to spatiotemporal water content distribution. However, at later times (as $t \to \infty$), V vanishes quickly, and $W(z)$, the steady state term, would be the solution. A plot of the analytical solution (Eq. (12)) is shown in Figure 5 for the following soil parameters:

$$\theta_0 = 0.3, \quad \theta_r = 0.0286, \quad \theta_s = 0.3658,$$

$$L = 100 \text{ cm}, \quad \alpha = 0.01\frac{1}{\text{cm}}, \quad K_s = 10^{-3}\frac{\text{cm}}{\text{s}}.$$

As shown, water content profiles reflect the unsteady infiltrating front with constant water contents at the top and bottom of the column ($\theta_0 = 0.3$ and $\theta_r = 0.0286$, respectively), which eventually ends up in a nonlinear (due to gravity) steady state. Obviously,

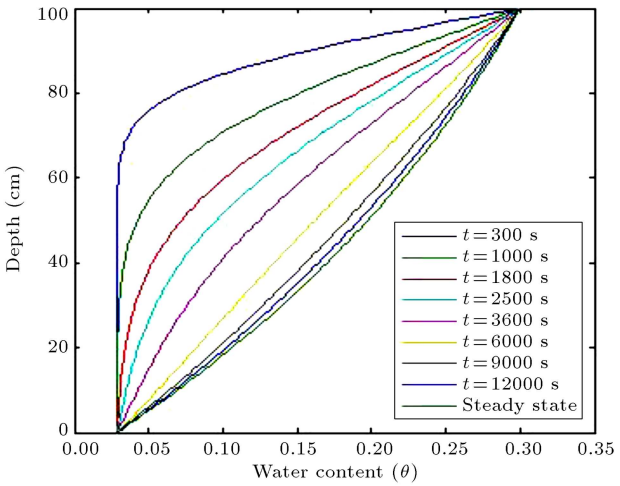

Figure 5. Water content distribution for the analytical solution (Eq. (12)) for various times.

as time elapses, the profiles approach steady state, and their temporal variation (advancement) approaches zero.

Figure 6(a) and (b) show comparisons of a Finite-Difference Method (FDM) solution (to Eq. (10)) by implicit scheme with the analytical solution for $t = 5$ min and $t = 10$ min, respectively. The FDM solution was obtained for $\Delta t = 1$ min and $\Delta z = 5$ cm. As shown, both solutions coincide well with one another.

A different boundary condition may be assumed for the 1D vertical water infiltration problem (Eq. (10)), whereby an initially "dried" soil column, $\theta(z,0) = \theta_r$, is subjected to a fixed water content at $z = 0$ and $z = L$; $\theta(0,t) = \theta(L,t) = \theta_0 > \theta_r$, thus allowing the column to imbibe water from both ends. Following similar mathematical procedure as before, the answer for $\theta(z,t)$ would be:

$$(z,t) = e^{-\frac{f}{2D}z-\frac{f^2}{4D}t}\sum_{n=1}^{\infty}\frac{2}{L}(\theta_r-\theta_0)$$

$$\frac{-e^{\frac{f}{2D}L}\left(\frac{n\pi}{L}\right)(-1)^n+\left(\frac{n\pi}{L}\right)}{\left(\frac{f}{2D}\right)^2+\left(\frac{n\pi}{L}\right)^2}\sin\left(\frac{n\pi}{L}z\right)$$

$$e^{-\left(\frac{n\pi}{L}\right)^2 Dt+\theta_0}. \tag{14}$$

Obviously, Eq. (14) satisfies Eq. (10) and the aforementioned boundary and initial conditions. The first term in the equation, the unsteady term, consists of two exponential expressions in t and z (with negative powers) in and out of an infinite series. It reflects the spatiotemporal water content distribution in the column above and over the fixed water content at both ends of the column, θ_0. Justifiably, it vanishes as $t \to \infty$ and only the second term in the equation, the steady term $W = \theta_0$, would be the solution. A plot of the solution (Eq. (14)) is shown in Figure 7 for the following soil parameters:

$$\theta_0 = 0.3, \quad \theta_r = 0.0286, \quad \theta_s = 0.3658,$$

$$L = 1000 \text{ cm}, \quad \alpha = 0.01\frac{1}{\text{cm}}, \quad K_s = 10^{-3}\frac{\text{cm}}{\text{s}}.$$

As shown in the figure, water content profiles reflect a combination of two unsteady fronts due to the high water content gradient at the top and bottom of the column. The first one is an infiltrating front from top to bottom, and the second is an imbibed front from bottom to top of the column. Perceptibly, gravity effect expedites advancement of the former and impedes that of the latter; an effect that makes the overall water content profiles asymmetric unless at the steady state where a constant water content (θ_0) is achieved throughout the column.

Figure 8(a) and (b) show comparisons of the Finite-Difference Method (FDM) solution to the problem by implicit scheme, with the analytical solution (Eq. (14)) for $t = 1000$ min and $t = 1500$ min, respectively. The FDM solution was obtained for

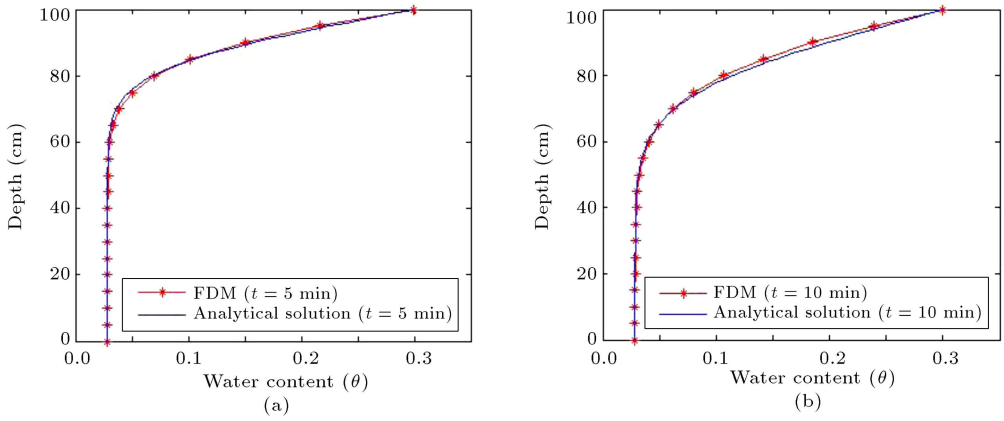

Figure 6. Comparison of water content profiles obtained by the analytical and FDM solutions to Eq. (10) for (a) $t = 5$ min and (b) $t = 10$ min.

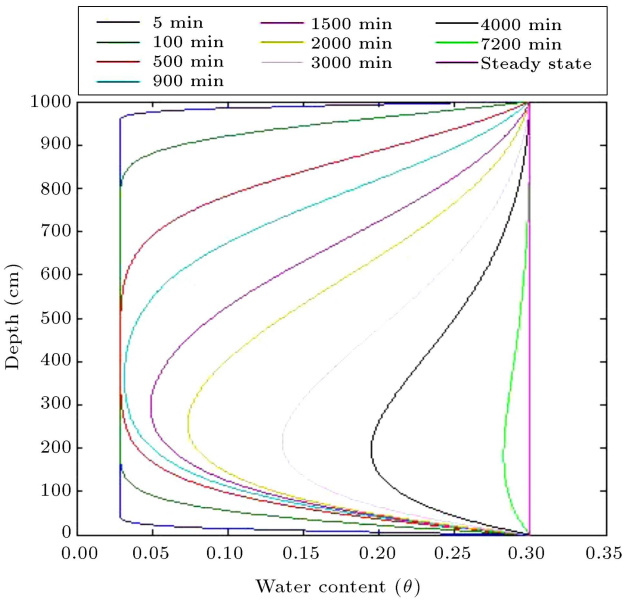

Figure 7. Water content profile at different times for the analytical solution presented in Eq. (14).

$\Delta t = 5$ min and $\Delta z = 10$ cm. As shown, both solutions coincide well with one another.

5. Analytical solution for 2D water infiltration

Richards' equation in a vertical 2D plane (x, z) may be expressed as (see Eq. (5)):

$$\frac{\partial \theta}{\partial t} = D\frac{\partial^2 \theta}{\partial z^2} + f\frac{\partial \theta}{\partial z} + D\frac{\partial^2 \theta}{\partial x^2}, \tag{15}$$

where D and f are defined before. If vertical water infiltration from the top edge of the plane is considered, then the initial and boundary conditions would be:

$$\theta(0, z, t) = \theta_r, \quad \theta(a, z, t) = \theta_r, \tag{16a}$$

$$\theta(x, 0, t) = \theta_r, \quad \theta(x, b, t) = \theta_0, \tag{16b}$$

$$\theta(x, z, 0) = \theta_r, \tag{16c}$$

where $\theta_0 > \theta_r$, and a schematic view of the problem statement is shown in Figure 9. A single closed form analytical solution is sought that encompasses both steady and unsteady solutions. Thus, the general form of such a solution may be expressed as a combination of a steady (W) and an unsteady (V) term:

$$\theta(x, z, t) = V(x, z, t) + w(x, z). \tag{17}$$

Obviously, non-homogenous boundary conditions are to satisfy $w(x, z)$, the steady solution, and homogenous boundary conditions are for $V(x, z, t)$, the unsteady solution. Substituting Eq. (17) into Eqs. (15) and (16a) to (16c) yields:

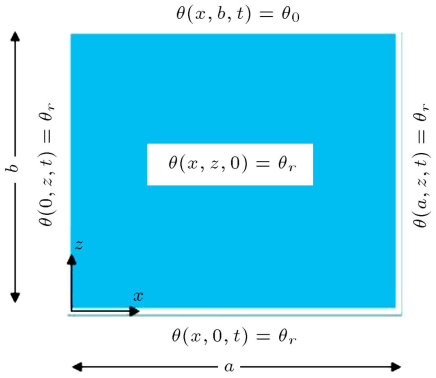

Figure 9. Schematic view of vertical infiltration in a 2D (x, z) plane.

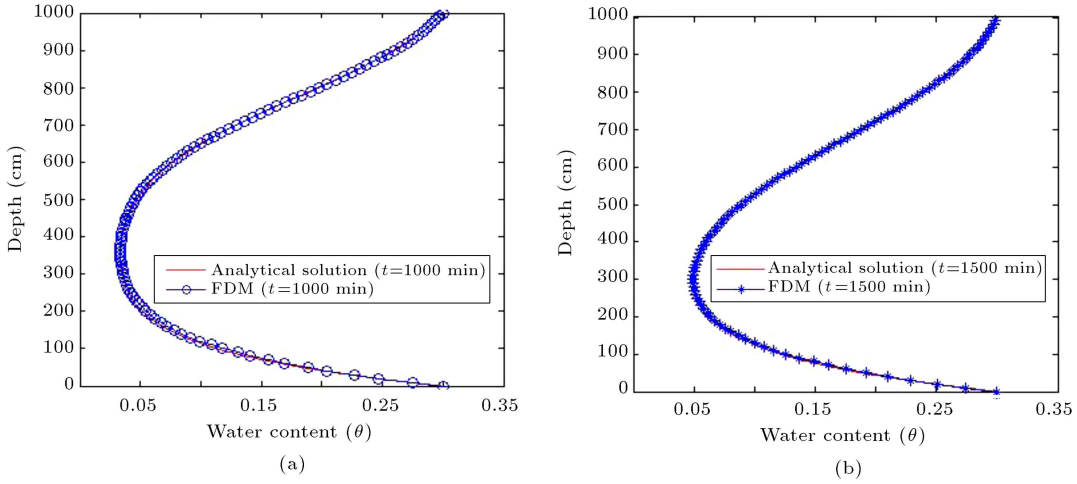

Figure 8. Comparison of water content profiles obtained by the analytical (Eq. (14)) and FDM solutions for (a) $t = 1000$ min and (b) $t = 1500$ min.

$$D\frac{\partial^2 V}{\partial z^2}+f\frac{\partial V}{\partial z}+D\frac{\partial^2 V}{\partial x^2}-\frac{\partial V}{\partial t}=0, \tag{18a}$$

$$V(x,0,t)=0 \quad V(x,b,t)=0, \tag{18b}$$

$$V(0,z,t)=0 \quad V(a,z,t)=0, \tag{18c}$$

$$V(x,z,0)=\theta_r-w(x,z). \tag{18d}$$

Similarly, the PDE for $w(x,z)$ may be written as:

$$D\frac{\partial^2 w}{\partial z^2}+f\frac{\partial w}{\partial z}+D\frac{\partial^2 w}{\partial x^2}=0, \tag{19a}$$

$$w(x,0)=\theta_r \quad w(x,b)=\theta_0, \tag{19b}$$

$$w(0,z)=\theta_r \quad w(a,z)=\theta_r. \tag{19c}$$

If $w(x,z)$ is assumed to have two components as follows:

$$w(x,z)=u(x,z)+q(z), \tag{20}$$

then, the PDE for $u(x,z)$ and $q(z)$ may be written as follows:

$$Dq''+fq'=0, \tag{21a}$$

$$q(b)=\theta_0, \quad q(0)=\theta_r, \tag{21b}$$

$$D\frac{\partial^2 u}{\partial z^2}+f\frac{\partial u}{\partial z}+D\frac{\partial^2 u}{\partial x^2}=0, \tag{22a}$$

$$u(x,0)=0, \quad u(x,b)=0, \tag{22b}$$

$$u(0,z)=\theta_r-q(z), \quad u(a,z)=\theta_r-q(z). \tag{22c}$$

By changing variable $u(x,z)=e^{-\frac{f}{2D}z}N(x,z)$ and utilizing separation of variables for $N(x,z)$, then $w(x,z)$ would be:

$$\begin{aligned} w(x,z)=&e^{-\frac{f}{2D}z}\sum_{n=1}^{\infty}\sin\left(\frac{n\pi}{b}z\right)\left[A_n\sinh(\sqrt{h+\lambda^2}x)\right.\\ &\left.+B_n\cosh(\sqrt{h+\lambda^2}x)\right]+\frac{\theta_r e^{-\frac{f}{D}b}-\theta_0}{-1+e^{-\frac{f}{D}b}}\\ &+\frac{(\theta_0-\theta_r)e^{-\frac{f}{D}z}}{-1+e^{-\frac{f}{D}b}}, \end{aligned} \tag{23}$$

where $\lambda=\frac{n\pi}{b}$, $n=1,2,3,...,\infty$, and $h=\frac{1}{4}\frac{f^2}{D^2}$. Also, A_n and B_n are defined as follows:

$$\begin{aligned} B_n=&\frac{2}{b}\int_0^b\left\{(\theta_r-P_1)e^{\frac{f}{2D}z}-Q_1.e^{-\frac{f}{2D}z}\right\}\\ &\sin\left(\frac{n\pi}{b}z\right)dz=\frac{2}{b}\left[(\theta_r-P_1)\right.\\ &.\frac{-e^{\frac{f}{2D}b}\left(\frac{n.\pi}{b}\right)(-1)^n+\left(\frac{n.\pi}{b}\right)}{\left(\frac{f}{2D}\right)^2+\left(\frac{n.\pi}{b}\right)^2}\\ &\left.-Q_1.\frac{-e^{-\frac{f}{2D}b}\left(\frac{n.\pi}{b}\right)(-1)^n+\left(\frac{n.\pi}{b}\right)}{\left(\frac{f}{2D}\right)^2+\left(\frac{n.\pi}{b}\right)^2}\right], \end{aligned} \tag{24a}$$

$$A_n=\frac{B_n}{\sinh(\sqrt{h+\lambda^2}a)}\left[1-\cosh(\sqrt{h+\lambda^2}a)\right], \tag{24b}$$

where P_1 and Q_1 are:

$$P_1=\frac{\theta_r e^{-\frac{f}{D}b}-\theta_0}{-1+e^{-\frac{f}{D}b}}, \quad Q_1=\frac{(\theta_0-\theta_r)}{-1+e^{-\frac{f}{D}b}}. \tag{25}$$

Utilizing separation of variables for $V(x,z,t)$ as follows:

$$V(x,z,t)=Z(z)X(x)T(t), \tag{26}$$

and substituting Eq. (26) into Eq. (18a), one would get:

$$\frac{X''}{X}=-\frac{Z''}{Z}-\frac{f}{D}\frac{Z'}{Z}+\frac{1}{D}\frac{T'}{T}=\mu, \tag{27}$$

where μ is an arbitrary constant. If $\mu<0$, say $\mu=-\lambda^2$, $\lambda>0$, then considering the boundary conditions of Eq. (18c), $X(x)$ in Eq. (27) may be written as:

$$X_i=A_i^*\sin(\lambda,x), \quad \lambda=\frac{i\pi}{a}, \quad i=1,2,3,...,\infty, \tag{28}$$

where A_i^* is a constant. Substituting $-\lambda^2$ into Eq. (27) for $\frac{X''}{X}$ yields:

$$-\frac{Z''}{Z}-\frac{f}{D}\frac{Z'}{Z}=-\lambda^2-\frac{1}{D}\frac{T'}{T}=\rho, \tag{29}$$

where ρ is an arbitrary constant. If $\rho\geq 0$, then a trivial solution to $Z(z)$ in Eq. (29) would be obtained. If $\rho<0$, say $\rho=-\beta^2-\left(\frac{f}{D}\right)^2\frac{1}{4}$, $\beta>0$, then applying the boundary condition of Eq. (18b) into Eq. (29) would yield $Z(z)$ as follows:

$$\begin{aligned} &Z_m=C_m^*e^{-\frac{f}{2D}z}\sin(\beta z), \quad \beta=\frac{m\pi}{b},\\ &m=1,2,3,...,\infty, \end{aligned} \tag{30}$$

where C_m^* is a constant. In addition, $T(t)$ into Eq. (29) becomes:

$$T = B^*_{mi} e^{-\left(\lambda^2+\beta^2+\left(\frac{f}{D}\right)^2\frac{1}{4}\right)Dt}, \tag{31}$$

where B^*_{mi} is a constant. Substituting Eqs. (28), (30), and (31) into Eq. (26) yields:

$$V(x,z,t) = \sum_{m=1}^{\infty}\sum_{i=1}^{\infty} C_{mi} e^{-\frac{f}{2D}z}\sin(\beta z) \sin(\lambda x) e^{-\left(\lambda^2+\beta^2+\left(\frac{f}{D}\right)^2\frac{1}{4}\right)Dt}, \tag{32}$$

where C_{mi} is $A^*_i C^*_m B^*_{mi}$. Substituting the boundary condition of Eq. (18d) into Eq. (32) and using Fourier series properties for Eq. (32), C_{mi} is calculated by Eq. (33) as shown in Box I, where A_m and B_m are identical to A_n and B_n in Eqs. (24a) and (24b), respectively. Substituting Eqs. (23) and (32) into Eq. (17), $\theta(x,z,t)$ would be:

$$\begin{aligned}\theta(x,z,t) = {} & \sum_{m=1}^{\infty}\sum_{i=1}^{\infty} C_{mi} e^{-\frac{f}{2D}z}\sin(\beta z)\sin(\lambda x) \\ & e^{-\left(\lambda^2+\beta^2+(\frac{f}{D}^2)\frac{1}{4}\right)Dt} + e^{-\frac{f}{2D}z} \\ & \cdot\sum_{n=1}^{\infty}\sin\left(\frac{n\pi}{b}z\right)\left[A_n\sinh(\sqrt{h+\lambda^2}x)\right. \\ & \left. + B_n\cosh\left(\sqrt{h+\lambda^2}x\right)\right] + \frac{(\theta_0-\theta_r).e^{-\frac{f}{D}z}}{-1+e^{-\frac{f}{D}b}} \\ & + \frac{\theta_r.e^{-\frac{f}{D}b}-\theta_0}{-1+e^{-\frac{f}{D}b}}.\end{aligned} \tag{34}$$

As seen, the equation consists of four terms: a function of (x,z,t), a function of (x,z), a function of z only, and a constant. As $t\to\infty$, the first term vanishes, and the rest of the terms remain as residuals or the steady state solution. Based on the equation, water content contours are drawn in Figure 10(a) to (d) for $t = 5, 15, 30,$ and 60 min, respectively. Figures are generated for the following soil parameters:

$$a = 100\text{ cm},\quad b = 100\text{ cm},\quad \theta_0 = 0.3,$$

$$\theta_r = 0.0286,\quad \theta_s = 0.365,$$

$$\alpha = 0.01\frac{1}{\text{cm}},\quad K_s = 10^{-3}\frac{\text{cm}}{\text{s}}.$$

Graphs in Figure 10 clearly show the infiltrating water content front that remains at $\theta_0 = 0.3$ at the top of soil sample ($z = 100$ cm) and at the residual value of $\theta_r = 0.0286$ at the bottom of the sample ($z = 0$). In addition, water content contours at $x = 0$ and $x = 100$ cm remain at $\theta_r = 0.0286$ all the times. 3D plots of water content, water depth, and water distance for $t = 30$ and 60 min (corresponding to Figure 10(c) and (d)) are visualized in Figure 11(a) and (b), respectively. Comparison of Figure 11(a) and (b) clearly depicts a 3D view of the infiltrating water content front.

6. Analytical solution for 2D water infiltration with no-flow on the side boundaries and a constant initial condition

Boundary and initial conditions may be applied to Eq. (15), such that a no-flow boundary condition is implemented on certain sides of the domain. No-flow

$$\begin{aligned}C_{mi} = {} & \frac{4}{ab}\int_0^a\int_0^b\left(\theta_r e^{\frac{f}{2D}z} - w(x,z)e^{\frac{f}{2D}z}\right)\sin(\beta z)\sin(\lambda x)dzdx \\ = {} & \frac{4}{ab}\left(-\frac{b}{2}\left(\frac{-A_m\left(\frac{i\pi}{a}\right)\sinh\left(\sqrt{h+\left(\frac{m\pi}{b}\right)^2}a\right)(-1)^i + B_m\left(\frac{i\pi}{a}\right)\left((-1)^{i+1}\cosh\left(\sqrt{h+\left(\frac{m\pi}{b}\right)^2}a\right)+1\right)}{h+\left(\frac{m\pi}{b}\right)^2+\left(\frac{i\pi}{a}\right)^2}\right)\right. \\ & - \frac{4\theta_r mba\left(-1+(-1)^i+e^{\frac{bf}{2D}}\left((-1)^m-(-1)^{m+i}\right)\right)}{\left(\left(\frac{fb}{D}\right)^2+4\pi^2m^2\right)i} \\ & \left. - \frac{4mba\left\{Q_1\left(1+(-1)^{i+1}\right)+P_1\left(1+(-1)^{i+1}\right)+Q_1e^{\frac{-bf}{2D}}\left((-1)^{m+1}+(-1)^{m+i}\right)+P_1e^{\frac{bf}{2D}}\left((-1)^{m+1}+(-1)^{m+i}\right)\right\}}{\left(\left(\frac{fb}{D}\right)^2+4\pi^2m^2\right)i}\right)\end{aligned} \tag{33}$$

Box I

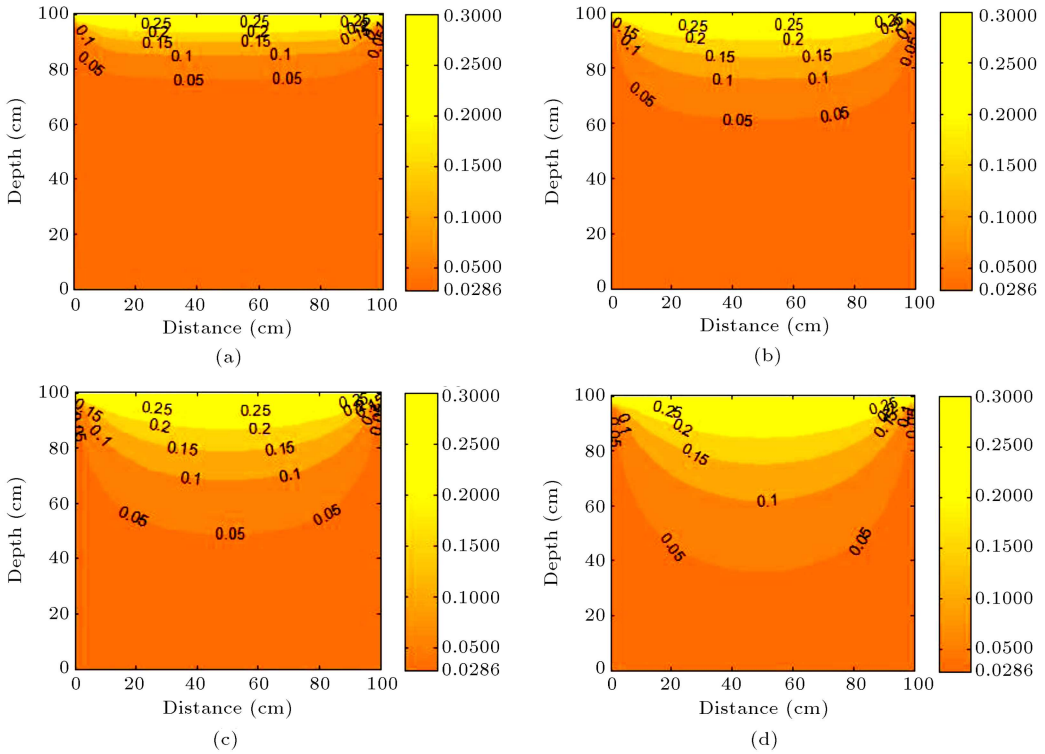

Figure 10. Water content contours based on the analytical solution to Eq. (34) for (a) $t = 5$ min, (b) $t = 15$ min, (c) $t = 30$ min, and (d) $t = 60$ min.

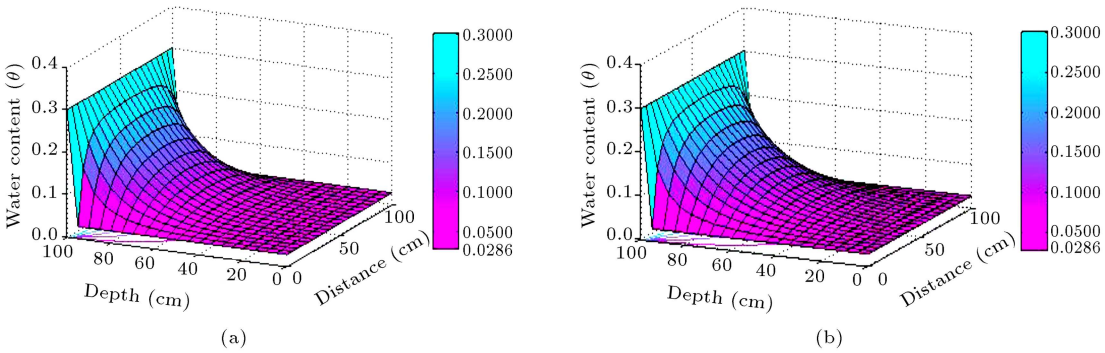

Figure 11. 3D plots of water content, water depth, water distance based on the analytical solution to Eq. (34) for (a) $t = 30$ min and (b) $t = 60$ min.

boundary conditions at $x = 0$ and $x = a$ and constant boundary conditions at $z = 0$ and $z = b$ along with a constant initial condition are mathematically written as follows:

$$\frac{\partial\theta}{\partial x}(0,z,t) = 0, \qquad \frac{\partial\theta}{\partial x}(a,z,t) = 0, \tag{35a}$$

$$\theta(x,0,t) = \theta_r, \qquad \theta(x,b,t) = \theta_0, \tag{35b}$$

$$\theta(x,z,0) = \theta_r. \tag{35c}$$

$\theta(x,z,t)$ may be divided into two terms as:

$$\theta(x,z,t) = V(x,z,t) + w(z). \tag{36}$$

Replacing Eq. (36) into Eqs. (15) and (35) and considering the non-homogenous boundary (Eq. (35b)) for $w(z)$, one would obtain:

$$w(z) = P_1 + Q_1 e^{-\frac{f}{D}z},$$

$$P_1 = \frac{\theta_r e^{-\frac{f}{D}b} - \theta_0}{-1 + e^{-\frac{f}{D}b}},$$

$$Q_1 = \frac{(\theta_0 - \theta_r)}{-1 + e^{-\frac{f}{D}b}}. \tag{37}$$

$V(x,z,t)$ may be expressed via separation of variables as follows:

$$V(x,z,t) = X(x)Z(z)T(t). \tag{38}$$

Substituting Eq. (38) into Eq. (15) and applying some simplifications gives:

$$\frac{X''}{X} = -\left(\frac{Z''}{Z} + \frac{f}{D}\frac{Z'}{Z} - \frac{1}{D}\frac{T'}{T}\right) = \mu, \tag{39}$$

where μ is an arbitrary constant. If $\mu = 0$ and $\mu < 0$, say $\mu = -\beta^2$ and $\beta > 0$, then $X(x)$ has two answer:

$$X = B, \tag{40}$$

$$X_n = A_n^* \cos(\beta x), \quad \beta = \frac{n\pi}{a}, \quad n = 1, 2, 3, ..., \infty, \tag{41}$$

where B and A_n^* are constants. Substituting $\mu = 0$ and $\mu = -\beta^2$ into Eq. (39) for $\frac{X''}{X}$, two equations are obtained:

$$-\beta^2 = -\left(\frac{Z''}{Z} + \frac{f}{D}\frac{Z'}{Z} - \frac{1}{D}\frac{T'}{T}\right), \tag{42a}$$

$$0 = -\left(\frac{Z''}{Z} + \frac{f}{D}\frac{Z'}{Z} - \frac{1}{D}\frac{T'}{T}\right). \tag{42b}$$

Considering Eqs. (35b) and (36), homogeneous boundaries for $V(x, z, t)$ based on Eq. (42a) gives:

$$Z_m = B_m^* e^{-\frac{f}{2D}z} \sin(vz), \quad v = \frac{m\pi}{b},$$

$$m = 1, 2, 3, ..., \infty, \tag{43}$$

$$T(t) = C_{mn}^* e^{-\left(\beta^2 + v^2 + \left(\frac{f}{D}\right)^2 \frac{1}{4}\right)Dt}, \tag{44}$$

where B_m^* and C_{mn}^* are constants. Substituting Eqs. (41), (43), and (44) into Eq. (38), an answer for $V(x, z, t)$ would be derived as:

$$V_1(x, z, t) = \sum_{m=1}^{\infty}\sum_{n=1}^{\infty} C_{mn} \cos\left(\frac{n\pi}{a}x\right) \sin\left(\frac{m\pi}{b}z\right) e^{-\frac{f}{2D}z} e^{-\left(\beta^2 + v^2 + \left(\frac{f}{D}\right)^2 \frac{1}{4}\right)Dt}, \tag{45}$$

where C_{mn} is $A_n^* B_m^* C_{mn}^*$.

A similar procedure may be followed to obtain $Z(z)$ and $T(t)$ in Eq. (42b):

$$Z_m = A_m^* e^{-\frac{f}{2D}z} \sin(\eta z), \quad \eta = \frac{m\pi}{b},$$

$$m = 1, 2, 3, ..., \infty, \tag{46}$$

$$T = B_i^* e^{-\left(\eta^2 + \left(\frac{f}{D}\right)^2 \frac{1}{4}\right)Dt}, \tag{47}$$

where A_m^* and B_i^* are constants. Substituting Eqs. (40), (46), and (47) into Eq. (38), another answer would be obtained for $V(x, z, t)$:

$$V_2(z, t) = \sum_{m=1}^{\infty} C_m e^{-\frac{f}{2D}z} \sin\left(\frac{m\pi}{b}z\right) e^{-\left(\eta^2 + \left(\frac{f}{D}\right)^2 \frac{1}{4}\right)Dt}, \tag{48}$$

where C_m is $BA_m^* B_i^*$. Now, $V(x, z, t)$ may be written as a combination of Eqs. (45) and (48):

$$V(x, z, t) = V_1(x, z, t) + V_2(z, t) = \sum_{m=1}^{\infty}\sum_{n=1}^{\infty} C_{mn} \cos\left(\frac{n\pi}{a}x\right) \sin\left(\frac{m\pi}{b}z\right) e^{-\frac{f}{2D}z} e^{-\left(\beta^2 + v^2 + \left(\frac{f}{D}\right)^2 \frac{1}{4}\right)Dt} + \sum_{m=1}^{\infty} C_m e^{-\frac{f}{2D}z} \sin\left(\frac{m\pi}{b}z\right) e^{-\left(\eta^2 + \left(\frac{f}{D}\right)^2 \frac{1}{4}\right)Dt}. \tag{49}$$

Substituting Eq. (36) into Eq. (35c) and replacing the result into Eq. (49), along with application of some Fourier series properties, would yield C_{mn} and C_m as follows:

$$C_{mn} = \frac{4}{ab}\int_0^b \int_0^a e\frac{f}{2D}z \left(\theta_r - P_1 - Q_1.e^{-\frac{f}{D}z}\right) \sin\left(\frac{m\pi}{b}z\right) \cos\left(\frac{n\pi}{a}x\right) dxdz \rightarrow C_{mn} = 0, \tag{50a}$$

$$C_m = \frac{2}{ab}\int_0^b \int_0^a e^{\frac{f}{2D}z} \left(\theta_r - P_1 - Q_1.e^{-\frac{f}{D}z}\right) \sin\left(\frac{m\pi}{b}z\right) dxdz = \frac{2}{b} .\left[(\theta_r - P_1).\frac{-e^{\frac{f}{2D}b}\left(\frac{m.\pi}{b}\right)(-1)^m + \left(\frac{m.\pi}{b}\right)}{\left(\frac{f}{2D}\right)^2 + \left(\frac{m.\pi}{b}\right)^2} - Q_1.\frac{-e^{\frac{-f}{2D}b}\left(\frac{m.\pi}{b}\right)(-1)^m + \left(\frac{m.\pi}{b}\right)}{\left(\frac{f}{2D}\right)^2 + \left(\frac{m.\pi}{b}\right)^2}\right]. \tag{50b}$$

Substituting Eqs. (49) and (37) into Eq. (36) gives:

$$\theta(x, z, t) = \sum_{m=1}^{\infty} C_m e^{-\frac{f}{2D}z} \sin\left(\frac{m\pi}{b}z\right) e^{-\left(\eta^2 + \left(\frac{f}{D}\right)\frac{1}{4}\right)Dt} + P_1 + Q_1.e^{-\frac{f}{D}z}. \tag{51}$$

Eq. (51) is independent of x and reflects a 1D vertical infiltration equation for z and t that is identical to Eq. (12) if $b = L$.

Figure 12(a) and (b) depict water content contours for Eq. (51) at $t = 900$ and 3600 s. Soil parameters used for the problem are identical to those used in Section 5. As shown, infiltrating front forms horizontal lines, which advance as the time increases until they reach the steady state (Figure 12(b)).

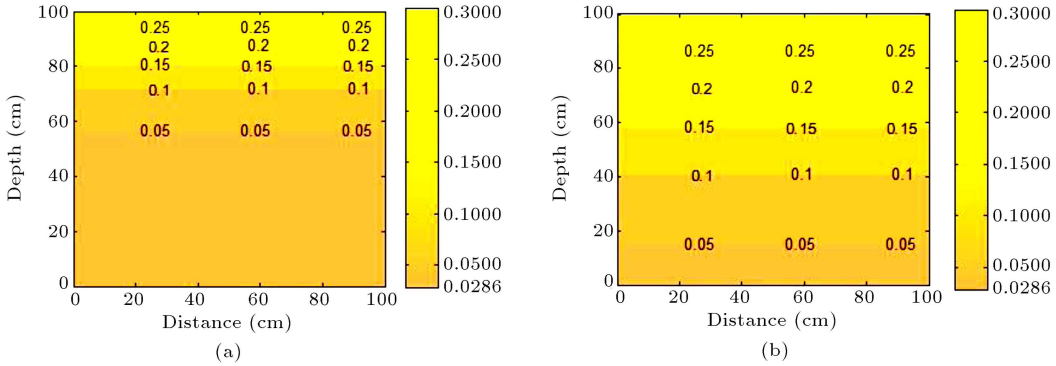

Figure 12. Vertically infiltrating water content contours plotted based on Eq. (51) for (a) $t = 900$ s and (b) $t = 3600$ s.

6.1. Analytical solution to 2D water infiltration with no-flow on the side boundaries and a sinusoidal initial condition

The only difference in this section (compared to the previous one) is the sinusoidal initial condition over the 2D domain, which may be mathematically expressed as:

$$\theta(x,z,0) = \theta_0 \sin\left(\frac{\pi x}{a}\right)\sin\left(\frac{\pi z}{b}\right). \tag{52}$$

Thus, initial condition for $V(x,z,0)$ would be:

$$V(x,z,0) = \theta_0 \sin\left(\frac{\pi x}{a}\right)\sin\left(\frac{\pi z}{b}\right) - w(z). \tag{53}$$

Substituting Eq. (53) into Eq. (49), C_{mn} may be calculated by Eq. (54) as shown in Box II. Also, C_m in Eq. (49) would be obtained by Eq. (55) as shown in Box III. Finally, substituting Eqs. (49) and (37) into Eq. (36) yields:

$$\theta(x,z,t) = \sum_{m=1}^{\infty}\sum_{n=1}^{\infty} C_{mn}\cos\left(\frac{n\pi}{a}x\right)\sin\left(\frac{m\pi}{b}z\right) e^{-\frac{f}{2D}z} e^{-\left(\beta^2+v^2+\left(\frac{f}{D}\right)^2\frac{1}{4}\right)Dt} + \sum_{m=1}^{\infty} C_m e^{-\frac{f}{2D}z}\sin\left(\frac{m\pi}{b}z\right) e^{-\left(\eta^2+\left(\frac{f}{D}\right)^2\frac{1}{4}\right)Dt} + Q_1.e^{-\frac{f}{D}z} + P_1. \tag{56}$$

The first two terms in Eq. (56) are functions of x, z and t, reflecting unsteady behavior of the infiltrating

$$C_{mn} = \frac{4}{ab}\int_0^b\int_0^a e^{\frac{f}{2D}z}\left(\theta_0\sin\left(\frac{\pi x}{a}\right)\sin\left(\frac{\pi z}{b}\right) - P_1 - Q_1.e^{-\frac{f}{D}z}\right)\cos\left(\frac{n\pi}{a}x\right)\sin\left(\frac{m\pi}{b}z\right)dxdz$$
$$= 8\theta_0\left(\frac{Hb\pi^2 m\left(1+e^{Hb}(-1)^m\right)}{H^4b^4+2H^2b^2\pi^2(1+m^2)+\pi^4-2\pi^4m^2+\pi^4m^4}\frac{(1+(-1)^n)}{\pi(n^2-1)}\right), \qquad \text{for } n \neq 1, \tag{54}$$

where $H = \frac{f}{2D}$ and $C_{mn} = 0$ if $n = 1$.

Box II

$$C_m = \frac{2}{ab}\int_0^b\int_0^a e^{\frac{f}{2D}z}\left(\theta_0\sin\left(\frac{\pi x}{a}\right)\sin\left(\frac{\pi z}{b}\right) - P_1 - Q_1.e^{-\frac{f}{D}z}\right)\sin\left(\frac{m\pi}{b}z\right)dxdz$$
$$= 2\left(\theta_0\frac{-2Hb\pi^2 m\left(1+e^{Hb}(-1)^m\right)}{H^4b^4+2H^2b^2\pi^2(1+m^2)+\pi^4-2\pi^4m^2+\pi^4m^4}\frac{2}{\pi} + P_1\frac{m\pi\left(-1+e^{Hb}(-1)^m\right)}{H^2b^2+m^2\pi^2} - Q_1\frac{m\pi\left(e^{Hb}-(-1)^m\right)e^{-Hb}}{H^2b^2+m^2\pi^2}\right). \tag{55}$$

Box III

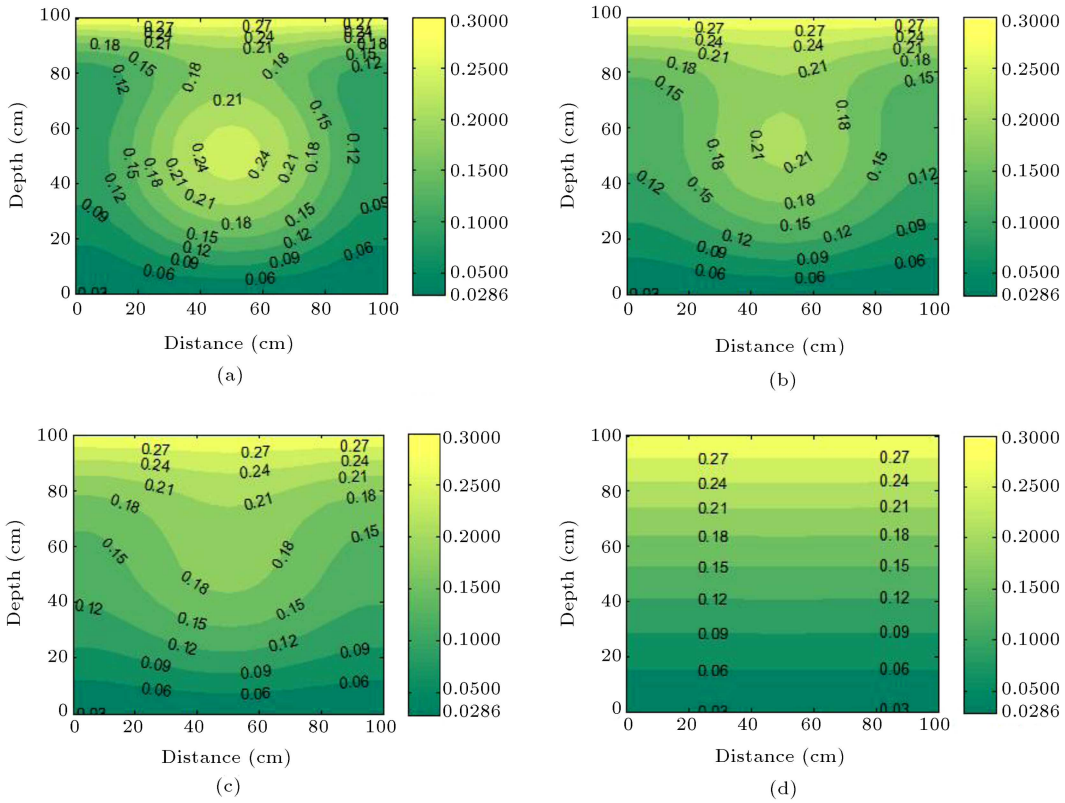

Figure 13. Water content contours for 2D water infiltration with no-flow on the side boundaries and a sinusoidal initial condition for (a) $t = 5$ min, (b) $t = 10$ min, (c) $t = 15$ min, and (d) $t = 60$ min.

water content front. However, the last two terms are not functions of time and reflect the steady behavior of the front. Obviously, as $t \to \infty$, the first two terms vanish and the solution approaches that of a 1D vertical steady infiltration presented by the last two terms in Eq. (12).

Figure 13(a) to (d) depict water content contours for equation Eq. (56) for $t = 5, 10, 15$ and 60 min, respectively. Soil parameters used for the problem are identical to those used in Section 5. At early times (Figure 13(a) and (b)) water content contours reflect a combination of two distinct water content gradients: 1) from center of the domain outward due to the sinusoidal initial bell shape gradient, and 2) from top to bottom (the infiltrating front) due to the gradient in water contents at top and bottom boundaries. As time elapses, the bell shape gradient attenuates, the 1D vertical infiltration prevails (Figure 13(c) and (d)), and eventually water content contours approach a steady state exponential profile associated with the last two terms in Eq. (56).

To illustrate the use of the derived equations, water content values from the analytical solution (Eq. (56)) is compared to an explicit scheme Finite Difference Method (FDM) solution (to Eq. (15) with boundary conditions (Eqs. (35a) and (35b)) and initial condition (Eq. (52))) in Tables 1-4. The soil properties for both solutions are:

$$a = 100 \text{ cm}, \quad b = 100 \text{ cm}, \quad \theta_0 = 0.3,$$

$$\theta_r = 0.0286, \quad \theta_s = 0.3658, \quad K_s = 10^{-3} \frac{\text{cm}}{\text{s}}.$$

The tables are for four α values of $0.01, 0.0075, 0.005$, and $0.0025 \ \frac{1}{\text{cm}}$, utilized by Tracy [16], too. The comparison is performed for $t = 30$ min, $x = 50$ cm, $z = 10$, 50 and 90 cm. The comparison is made for different numbers of grid point at x direction (N_x), z direction (N_z), and time steps (Δt). Relative Error (RE) defined as:

$$\text{RE} = \frac{|\theta_{\text{Analytical}} - \theta_{\text{Numerical}}|}{|\theta_{\text{Analytical}}|} \times 100\%,$$

was used as the index for comparison.

As expected, for all α 's, RE decreased considerably when N_x, and N_z increased (and the time step (Δt) decreased to guarantee numerical stability), such that for the highest number of grid points at x and z directions ($N_x = N_z = 101$) RE is less than 2%. However, as α increased, RE increased, too. Spatially, for all α's, RE at $z = 50$ cm was less than that at $z = 10$ and 90 cm for almost all N_x and N_z values. Apparently, to lower RE at $z = 10$ and 90 cm, it is necessary to refine the grids near top and bottom boundaries. Similar trends were observed by Tracy [16] for h-based Richards' equation. As he stated, these

Table 1. Comparisons of analytical with FDM solutions for various Z's at $x = 50$ cm, $t = 30$ min, and $\alpha = 0.0025 \frac{1}{\text{cm}}$.

$\alpha = 0.0025 \frac{1}{\text{cm}}$			$Z = 10$ cm			$Z = 50$ cm			$Z = 90$ cm		
N_x	N_z	Δt	$\theta_{\text{Analytical}}$	θ_{FDM}	RE (%)	$\theta_{\text{Analytical}}$	θ_{FDM}	RE (%)	$\theta_{\text{Analytical}}$	θ_{FDM}	RE (%)
11	11	10 s	0.0577	0.0528	8.49	0.1692	0.1562	7.68	0.2747	0.2501	8.95
21	21	3 s	0.0577	0.0532	7.79	0.1692	0.1574	6.97	0.2747	0.2564	6.66
41	41	1 s	0.0577	0.0561	2.77	0.1692	0.1643	2.89	0.2747	0.2646	3.67
101	101	0.1 s	0.0577	0.0569	1.38	0.1692	0.1672	1.18	0.2747	0.2708	1.41

Table 2. Comparisons of analytical with FDM solutions for various Z's at $x = 50$ cm, $t = 30$ min, and $\alpha = 0.005 \frac{1}{\text{cm}}$.

$\alpha = 0.005 \frac{1}{\text{cm}}$			$Z = 10$ cm			$Z = 50$ cm			$Z = 90$ cm		
N_x	N_z	Δt	$\theta_{\text{Analytical}}$	θ_{FDM}	RE (%)	$\theta_{\text{Analytical}}$	θ_{FDM}	RE (%)	$\theta_{\text{Analytical}}$	θ_{FDM}	RE (%)
11	11	10 s	0.0586	0.0514	12.28	0.1680	0.1534	8.69	0.2741	0.2481	9.48
21	21	5 s	0.0586	0.0534	8.87	0.1680	0.1553	7.55	0.2741	0.2534	7.55
41	41	2.5 s	0.0586	0.0568	3.07	0.1680	0.1624	3.33	0.2741	0.2621	4.37
101	101	0.3 s	0.0586	0.0577	1.53	0.1680	0.1656	1.42	0.2741	0.2695	1.67

Table 3. Comparisons of analytical with FDM solutions for various Z's at $x = 50$ cm, $t = 30$ min, and $\alpha = 0.0075 \frac{1}{\text{cm}}$.

$\alpha = 0.0075 \frac{1}{\text{cm}}$			$Z = 10$ cm			$Z = 50$ cm			$Z = 90$ cm		
N_x	N_z	Δt	$\theta_{\text{Analytical}}$	θ_{FDM}	RE (%)	$\theta_{\text{Analytical}}$	θ_{FDM}	RE (%)	$\theta_{\text{Analytical}}$	θ_{FDM}	RE (%)
11	11	10 s	0.0618	0.0501	18.93	0.1685	0.1521	9.73	0.2725	0.2414	11.41
21	21	5 s	0.0618	0.0534	13.59	0.1685	0.1548	8.13	0.2725	0.2501	8.22
41	41	2.5 s	0.0618	0.0581	5.98	0.1685	0.1596	5.28	0.2725	0.2591	4.91
101	101	0.5 s	0.0618	0.0608	1.61	0.1685	0.1656	1.72	0.2725	0.2676	1.79

Table 4. Comparisons of analytical with FDM solutions for various Z's at $x = 50$ cm, $t = 30$ min, and $\alpha = 0.01 \frac{1}{\text{cm}}$.

$\alpha = 0.01 \frac{1}{\text{cm}}$			$Z = 10$ cm			$Z = 50$ cm			$Z = 90$ cm		
N_x	N_z	Δt	$\theta_{\text{Analytical}}$	θ_{FDM}	RE (%)	$\theta_{\text{Analytical}}$	θ_{FDM}	RE (%)	$\theta_{\text{Analytical}}$	θ_{FDM}	RE (%)
11	11	10 s	0.0669	0.0498	25.56	0.1716	0.1521	11.36	0.2706	0.2331	13.85
21	21	5 s	0.0669	0.0574	14.20	0.1716	0.1546	9.90	0.2706	0.2421	10.53
41	41	5 s	0.0669	0.0616	7.92	0.1716	0.1603	6.58	0.2706	0.2538	6.20
101	101	0.5 s	0.0669	0.0656	1.94	0.1716	0.1684	1.86	0.2706	0.2653	1.95

results demonstrate the usefulness of having analytical solutions to test numerical programs.

7. Analytical solution for 3D water infiltration

Richards' equation for 3D water infiltration in an isotropic homogeneous Cartesian coordinate system is (see Eq. (5)):

$$\frac{\partial \theta}{\partial t} = D\frac{\partial^2 \theta}{\partial x^2} + D\frac{\partial^2 \theta}{\partial y^2} + D\frac{\partial^2 \theta}{\partial z^2} + f\frac{\partial \theta}{\partial z}, \tag{57}$$

where D and f are defined earlier. A rectangular cube may be considered as the domain. Water infiltration would be triggered by a constant but higher water content on the top surface of the cube compared to the remainder of the domain. Boundary and initial conditions for such a case would be:

$$\theta(0, y, z, t) = \theta_r, \quad \theta(a, y, z, t) = \theta_r, \tag{58a}$$

$$\theta(x, 0, z, t) = \theta_r, \quad \theta(x, b, z, t) = \theta_r, \tag{58b}$$

$$\theta(x, y, 0, t) = \theta_r, \quad \theta(x, y, L, t) = \theta_0, \tag{58c}$$

$$\theta(x, y, z, 0) = \theta_r. \tag{58d}$$

A schematic view of the problem statement is shown in Figure 14.

$\theta(x, y, z, t)$ may be considered as a combination of two terms: a steady (w) and an unsteady (V) one:

$$\theta(x, y, z, t) = V(x, y, z, t) + w(x, y, z). \tag{59}$$

As mentioned, the non-homogeneous boundary conditions are satisfied by $w(x, y, z)$, the steady state

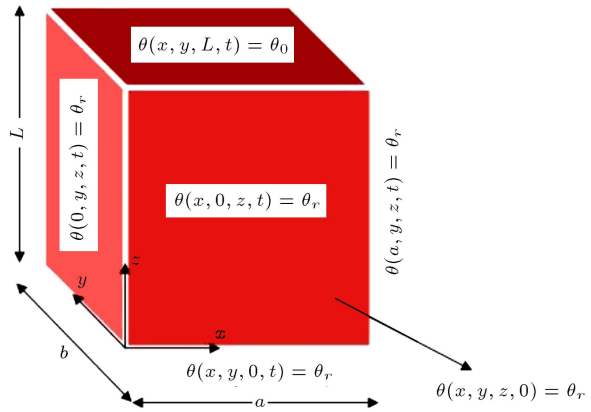

Figure 14. Schematic view of 3D infiltration problem in a cubical domain.

term, and homogeneous boundary conditions are set for $V(x,y,z,t)$, the unsteady state term. Substituting Eq. (59) into Eq. (57) and Eq. (58a) to Eq. (58d) yields:

$$D\frac{\partial^2 V}{\partial z^2}+f\frac{\partial V}{\partial z}+D\frac{\partial^2 V}{\partial x^2}+D\frac{\partial^2 V}{\partial y^2}-\frac{\partial V}{\partial t}=0, \quad (60a)$$

$$V(0,y,z,t)=0 \quad V(a,y,z,t)=0, \quad (60b)$$

$$V(x,0,z,t)=0 \quad V(x,b,z,t)=0, \quad (60c)$$

$$V(x,y,0,t)=0 \quad V(x,y,L,t)=0, \quad (60d)$$

$$V(x,y,z,0)=\theta_r-w(x,y,z), \quad (60e)$$

and:

$$D\frac{\partial^2 w}{\partial z^2}+f\frac{\partial w}{\partial z}+D\frac{\partial^2 w}{\partial x^2}+D\frac{\partial^2 w}{\partial y^2}=0, \quad (61a)$$

$$w(0,y,z)=\theta_r \quad w(a,y,z)=\theta_r, \quad (61b)$$

$$w(x,0,z)=\theta_r \quad w(x,b,z)=\theta_r, \quad (61c)$$

$$w(x,y,0)=\theta_r \quad w(x,y,L)=\theta_0. \quad (61d)$$

If $w(x,y,z)$ is, in turn, considered as two separate terms:

$$w(x,y,z)=u(x,y,z)+N(x,y), \quad (62)$$

then, substitution of Eq. (62) into Eqs. (61a) to (61d) yields:

$$\frac{\partial^2 N}{\partial x^2}+\frac{\partial^2 N}{\partial y^2}=0, \quad (63a)$$

$$N(0,y)=\theta_r \quad N(a,y)=\theta_r, \quad (63b)$$

$$N(x,0)=\theta_r \quad N(x,b)=\theta_r. \quad (63c)$$

As a simple example for the solution to Eqs. (63a) to (63c), one may consider $N(x,y)=\theta_r$.

Also, the partial differential equation for $u(x,y,z)$ would be written as:

$$D\frac{\partial^2 u}{\partial z^2}+f\frac{\partial u}{\partial z}+D\frac{\partial^2 u}{\partial x^2}+D\frac{\partial^2 u}{\partial y^2}=0, \quad (64a)$$

$$u(0,y,z)=0 \quad u(a,y,z)=0, \quad (64b)$$

$$u(x,0,z)=0 \quad u(x,b,z)=0, \quad (64c)$$

$$u(x,y,0)=0 \quad u(x,y,L)=\theta_0-\theta_r=\theta_r'. \quad (64d)$$

Applying separation of variables to $u(x,y,z)$:

$$u(x,y,z)=X(x)Y(y)Z(z), \quad (65)$$

and substituting Eq. (65) into Eq. (64a), while using Eqs. (64b) and (64c) we obtain:

$$Y_n=A_n^*\sin(\lambda y), \quad \lambda=\frac{n\pi}{b}, \quad n=1,2,3,\ldots,\infty, \quad (66)$$

$$X_m=B_m^*\sin(\beta x), \quad \beta=\frac{m.\pi}{a}, \quad m=1,2,3,\ldots,\infty, \quad (67)$$

where A_n^* and B_m^* are constants. Similarly, $Z(z)$ in Eq. (65) becomes:

$$Z=e^{-\frac{fz}{2D}}\left(C_1^*e^{\tau z}+C_2^*e^{-\tau z}\right),$$

$$\tau=\sqrt{\frac{1}{4}\left(\frac{f}{D}\right)^2+(\beta^2+\lambda^2)}, \quad (68)$$

where C_1^* and C_2^* are constants. Eq. (68) may be further simplified as:

$$Z=C_{mn}^*e^{-\frac{fz}{2D}}\sinh(\tau z)+B_{mn}^*e^{-\frac{fz}{2D}}\cosh(\tau z). \quad (69)$$

Applying the boundary condition of Eq. (64d), $u(x,y,0)=0$ to Eq. (69) gives:

$$Z=C_{mn}^*e^{-\frac{fz}{2D}}\sinh(\tau z), \quad (70)$$

where C_{mn}^* is a constant. Substituting Eqs. (66), (67), and (70) into Eq. (65) would give:

$$u(x,y,z)=\sum_{m=1}^{\infty}\sum_{n=1}^{\infty}C_{mn}e^{-\frac{f}{2D}z}\sinh(\tau z)\sin(\beta x)\sin(\lambda y), \quad (71)$$

where C_{mn} is $A_n^*B_m^*C_{mn}^*$. Now, using Eq. (64d)

$u(x,y,L)=\theta_0-\theta_r=\theta'_r$ and Fourier series properties, C_{mn} in Eq. (71) would be obtained as:

$$C_{mn}=\frac{4}{ab}\int_0^b\int_0^a\frac{\theta'_r e^{\frac{f}{2D}L}}{\sinh(\tau L)}\sin(\beta x)\sin(\lambda y)dxdy$$
$$=\frac{4\theta'_r e^{\frac{f}{2D}L}}{\sinh(\tau L)}\frac{\left(1-(-1)^n-(-1)^m+(-1)^{m+n}\right)}{mn\pi^2}. \quad (72)$$

As stated in Eq. (62), one may readily add up Eq. (71) and $N(x,y)=\theta_r$, to get $w(x,y,z)$.

Separation of variables may also be applied to $V(x,y,z,t)$ in Eq. (60):

$$V(x,y,z,t)=X(x)Y(y)Z(z)T(t). \quad (73)$$

Substituting Eq. (73) in Eq. (60a), simplification, and applying Eqs. (60b), (60c) and (60d) one would obtain:

$$X_i=A_i^*\sin(\beta x),\quad \beta=\frac{i.\pi}{a}\quad i=1,2,3,...,\infty, \quad (74a)$$

$$Y_i=B_j^*\sin(\eta y),\quad \eta=\frac{j.\pi}{b}\quad j=1,2,3,...,\infty, \quad (74b)$$

$$Z_k=C_k^* e^{-\frac{f}{2D}z}\sin(vz),\quad v=\frac{k\pi}{L},$$
$$k=1,2,3,...,\infty, \quad (74c)$$

$$T=F_{ijk}^* e^{-\left(\eta^2+\beta^2+v^2+(\frac{f}{D})^2\frac{1}{4}\right)Dt}, \quad (74d)$$

where A_i^*, B_j^*, C_k^*, and F_{ijk}^* are constants. Substituting Eqs. (74a), (74b), (74c) and (74d) into Eq. (73) gives:

$$V(x,y,z,t)=\sum_{i=1}^{\infty}\sum_{j=1}^{\infty}\sum_{k=1}^{\infty}C_{ijk}\sin\left(\frac{i\pi}{a}x\right)\sin\left(\frac{j\pi}{b}y\right)$$
$$\sin\left(\frac{k\pi}{L}z\right)e^{-\frac{f}{2D}z}e^{-\left(\eta^2+\beta^2+v^2+(\frac{f}{D})^2\frac{1}{4}\right)Dt}, \quad (75)$$

where C_{ijk} is $A_i^*B_j^*C_k^*F_{ijk}^*$. Substituting the initial condition of Eq. (60e) into Eq. (75) and considering Fourier series properties, C_{ijk} may be obtained as:

$$C_{ijk}=\frac{8}{abL}\int_0^L\int_0^b\int_0^a\left(\theta_r e^{\frac{f}{2D}z}-w(x,y,z)e^{\frac{f}{2D}z}\right)$$
$$\sin\left(\frac{i\pi}{a}x\right)\sin\left(\frac{j\pi}{b}y\right)\sin\left(\frac{k\pi}{L}z\right)dxdydz$$
$$=\frac{2}{L}\times C_{ij}^*\times\frac{\left(\frac{k\pi}{L}\right)(-1)^k\sinh(\delta L)}{\delta^2+\left(\frac{k\pi}{L}\right)^2}, \quad (76)$$

where δ and C_{ij}^* are defined as:

$$\delta=\sqrt{\frac{1}{4}\left(\frac{f}{D}\right)^2+\left(\frac{i\pi}{a}\right)^2+\left(\frac{j\pi}{b}\right)^2}, \quad (77)$$

$$C_{ij}^*=\frac{4\theta'_r e^{\frac{f}{2D}L}}{\sinh(\delta L)}\frac{\left(1-(-1)^j-(-1)^i+(-1)^{j+i}\right)}{ji\pi^2}. \quad (78)$$

Substituting Eqs. (62) and (75) into Eq. (59) yields:

$$\theta(x,y,z,t)=\sum_{i=1}^{\infty}\sum_{j=1}^{\infty}\sum_{k=1}^{\infty}C_{ijk}\sin\left(\frac{i\pi}{a}x\right)\sin\left(\frac{j\pi}{b}y\right)$$
$$\sin\left(\frac{k\pi}{L}z\right)e^{-\frac{f}{2D}z}e^{-\left(\eta^2+\beta^2+v^2+(\frac{f}{D})^2\frac{1}{4}\right)Dt}$$
$$+\sum_{m=1}^{\infty}\sum_{n=1}^{\infty}C_{mn}e^{-\frac{f}{2D}z}\sinh(\tau z)\sin\left(\frac{m\pi}{a}x\right)$$
$$\sin\left(\frac{n\pi}{b}y\right)+\theta_r, \quad (79)$$

which gives the spatiotemporal variations of water content in the cube of Figure 14, and is considered as the exact analytical solution for Eq. (57). All boundary and initial conditions of Eqs. (58a) to (58d), as well as Eq. (57), are satisfied by Eq. (79). The first term in Eq. (79) is the unsteady state term, it vanishes as $t\to\infty$ (due to the second exponential expression), and the second and third terms remain as the residual or steady state terms. Problem statement dictates symmetrical water content profiles over two sections of 1) $x=a/2$ and 2) $y=b/2$; a fact that is incorporated in Eq. (79) due to the sinusoidal x and y terms. Furthermore, as the higher water content contours infiltrate into the cube as a "front", maximum advancement of the "front" always lays along the line of $(a/2,b/2,z)$.

To plot numerical examples for Eq. (79), the following soil parameters were selected:

$$a=100\text{ cm},\quad b=100\text{ cm},\quad L=100\text{ cm},$$
$$\theta_0=0.3,\quad \theta_r=0.0286,\quad \theta_s=0.3658,$$
$$\alpha=0.01\frac{1}{\text{cm}},\quad K_s=10^{-3}\frac{\text{cm}}{\text{s}}.$$

Figure 15(a) to (f) depict two dimensional (x,z) water content contours at vertical sections of $y=10,25$ and 50 cm at $t=15$ and 60 min. As shown, the boundary conditions of Eq. (58a) to (58c) are all satisfied; $\theta_r=0.0286$ is fixed at $x=0,100$ cm and $z=0$ cm and $\theta_0=0.3$ fixed at $z=100$ cm. Comparing figures for $t=15$ min (Figure 15(a), (c),

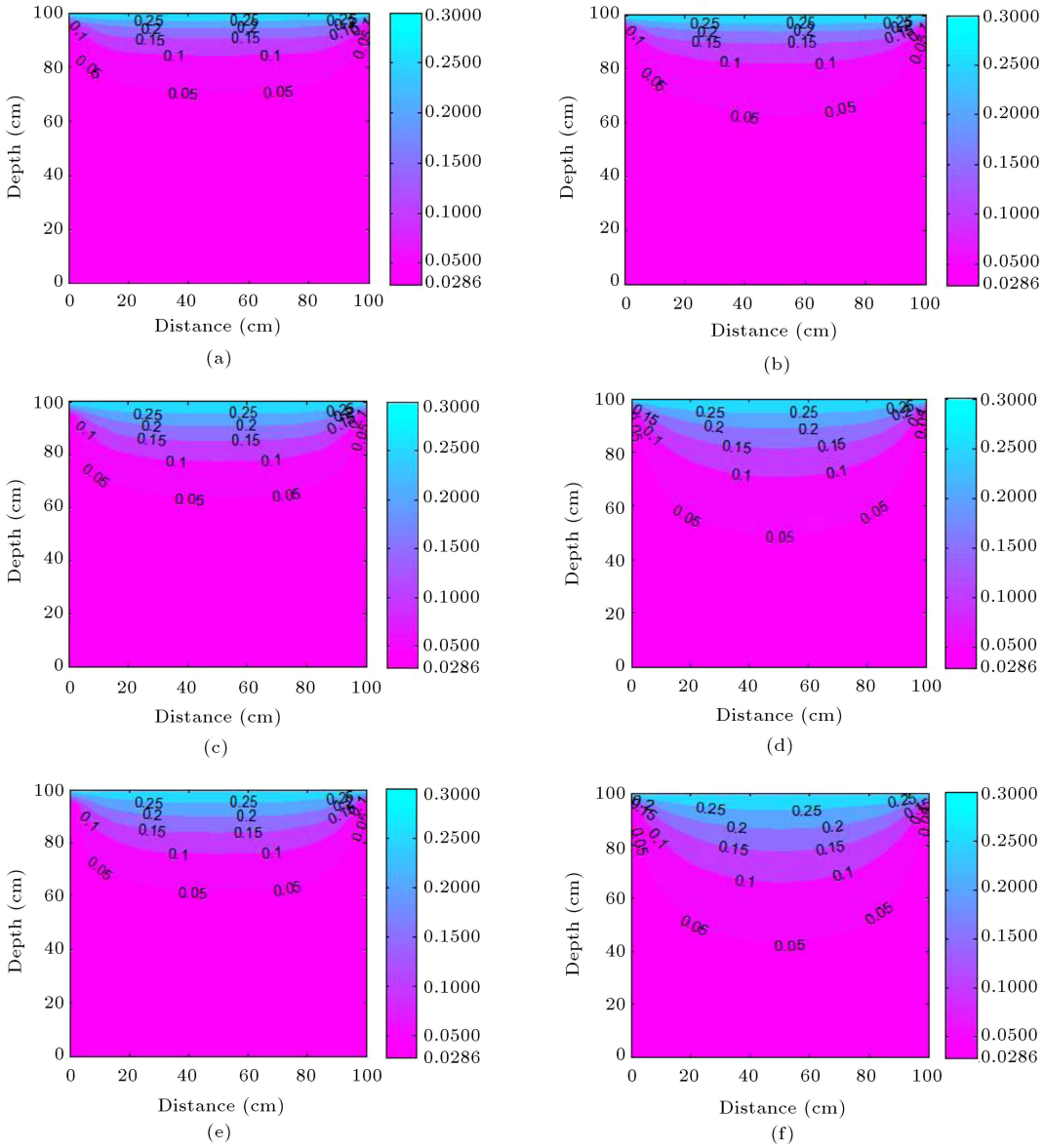

Figure 15. Water content contours for the 3D analytical solution presented in Eq. (79) for (a) $y = 10$ cm and $t = 15$ min, (b) $y = 10$ cm and $t = 60$ min, (c) $y = 25$ cm and $t = 15$ min, (d) $y = 25$ cm and $t = 60$ min, (e) $y = 50$ cm and $t = 15$ min, (f) $y = 50$ cm and $t = 60$ min.

and (e)) to those for $t = 60$ min (Figure 15(b), (d), and (f)), clearly shows temporal advancement of the vertically infiltrating front of water content from top ($z = 100$ cm) to bottom ($z = 0$ cm) of the cube at different sections. Comparing figures for $y = 10, 25$, and 50 cm reflects the fact that at higher y values (sections closer to the center of the cube), deeper infiltration of water content contours occurs, with the maximum advancement laying on the vertical line passing through the center of the cube. Finally, it was noted that at $t = 60$ min, contribution of the first, compared to the second and third terms in Eq. (79) was negligible; as if steady state was reached at this time.

8. Analytical solution for 3D water infiltration with no-flow on the side boundaries and a constant initial condition

Different boundary and initial conditions may be considered for Eq. (57). For example, no-flow may be considered on the side boundaries with higher water content on the top surface of the cube (compared to the remainder of the domain) triggering vertical infiltration of water content. Mathematical expression for such boundary and initial conditions would be:

$$\frac{\partial\theta}{\partial x}(0, y, z, t) = 0, \quad \frac{\partial\theta}{\partial x}(a, y, z, t) = 0, \tag{80a}$$

$$\frac{\partial\theta}{\partial y}(x,0,z,t)=0, \quad \frac{\partial\theta}{\partial y}(x,b,z,t)=0, \tag{80b}$$

$$\theta(x,y,0,t)=\theta_r, \quad \theta(x,y,L,t)=\theta_0, \tag{80c}$$

$$\theta(x,y,z,0)=\theta_r. \tag{80d}$$

As before, $\theta(x,y,z,t)$ is considered as:

$$\theta(x,y,z,t)=V(x,y,z,t)+w(z). \tag{81}$$

Substituting Eq. (81) into Eq. (57) and applying the boundary condition of Eq. (80c), $w(z)$ becomes:

$$w(z)=P+Qe^{-\frac{f}{D}z}, \quad P=\frac{\theta_r.e^{-\frac{f}{D}L}-\theta_0}{-1+e^{-\frac{f}{D}L}},$$

$$Q=\frac{(\theta_0-\theta_r)}{-1+e^{-\frac{f}{D}L}}. \tag{82}$$

The PDE for $V(x,y,z,t)$ is the same as Eq. (60a), however, with different boundary and initial conditions:

$$\frac{\partial V}{\partial x}(0,y,z,t)=0, \quad \frac{\partial V}{\partial x}(a,y,z,t)=0, \tag{83a}$$

$$\frac{\partial V}{\partial y}(x,0,z,t)=0, \quad \frac{\partial V}{\partial y}(x,b,z,t)=0, \tag{83b}$$

$$V(x,y,0,t)=0, \quad V(x,y,L,t)=0, \tag{83c}$$

$$V(x,y,z,0)=\theta_r-w(z), \tag{83d}$$

$V(x,y,z,t)$ may be separated as:

$$V(x,y,z,t)=X(x)Y(y)Z(z)T(t). \tag{84}$$

Substituting Eq. (84) into Eq. (60a) and applying some simplifications give:

$$\frac{X''}{X}=-\left(\frac{Z''}{Z}+\frac{f}{D}\frac{Z'}{Z}+\frac{Y''}{Y}-\frac{1}{D}\frac{T'}{T}\right)=\mu, \tag{85}$$

where μ is an arbitrary constant. If $\mu=0$ and $\mu<0$, say $\mu=-\beta^2$, $\beta>0$ then $X(x)$ in Eq. (85) has two answers as:

$$X_1=B, \tag{86}$$

$$X_n=A_n^*\cos(\beta x), \quad \beta=\frac{n.\pi}{a}, \qquad n=1,2,3,...,\infty, \tag{87}$$

where B and A_n^* are constants. If $\mu>0$, then a trivial solution would be obtained for $X(x)$. Substituting $\mu=0$ and $\mu=-\beta^2$ in Eq. (85) for $\frac{X''}{X}$, two equations are obtained:

$$-\beta^2=-\left(\frac{Z''}{Z}+\frac{f}{D}\frac{Z'}{Z}+\frac{Y''}{Y}-\frac{1}{D}\frac{T'}{T}\right), \tag{88a}$$

$$0=-\left(\frac{Z''}{Z}+\frac{f}{D}\frac{Z'}{Z}+\frac{Y''}{Y}-\frac{1}{D}\frac{T'}{T}\right). \tag{88b}$$

With rearrangements, Eq. (88a) becomes:

$$\beta^2-\left(\frac{Z''}{Z}+\frac{f}{D}\frac{Z'}{Z}-\frac{1}{D}\frac{T'}{T}\right)=\frac{Y''}{Y}=\rho, \tag{89}$$

where ρ is arbitrary constant. Applying $\rho=0$ and $\rho<0$, say $\rho=-\eta^2$, $\eta>0$ and boundary conditions of Eq. (83b), two answers for $Y(y)$ are obtained:

$$Y_1=D, \tag{90}$$

$$Y_m=B_m^*\cos(\eta y), \quad \eta=\frac{m.\pi}{b}, \quad m=1,2,3,...,\infty, \tag{91}$$

where D and B_m^* are constants. Substituting $\rho=0$ and $\rho=-\eta^2$ into Eq. (89) for $\frac{Y''}{Y}$, two equations may be written as:

$$\beta^2-\left(\frac{Z''}{Z}+\frac{f}{D}\frac{Z'}{Z}-\frac{1}{D}\frac{T'}{T}\right)=-\eta^2, \tag{92a}$$

$$\beta^2-\left(\frac{Z''}{Z}+\frac{f}{D}\frac{Z'}{Z}-\frac{1}{D}\frac{T'}{T}\right)=0. \tag{92b}$$

Using Eq. (83c) for Eq. (92a) gives:

$$Z_k^*=C_k^*e^{-\frac{f}{2D}z}\sin(\gamma z), \quad \gamma=\frac{k\pi}{L},$$

$$k=1,2,3,...,\infty, \tag{93}$$

$$T_{mnk}=D_{mnk}^*e^{-\left(\beta^2+\eta^2+\gamma^2+(\frac{f}{D})^2\frac{1}{4}\right)Dt}, \tag{94}$$

where C_k^* and D_{mnk}^* are constants. As before, Eq. (92b) yields:

$$Z_k^{**}=C_k^{**}e^{-\frac{f}{2D}z}\sin(\gamma z), \quad \gamma=\frac{k\pi}{L},$$

$$k=1,2,3,...,\infty, \tag{95a}$$

$$T_{nk}=E_{nk}^*e^{-\left(\beta^2+\gamma^2+(\frac{f}{D})^2\frac{1}{4}\right)Dt}, \tag{95b}$$

where C_k^{**} and E_{nk}^* are constants. Now, substituting Eqs. (87), (91), (93) and (94) into Eq. (84), the first answer for $V(x,y,z,t)$ yields as:

$$V_2(x,y,z,t)=X_n(x)Y_1(y)Z_k^{**}(z)T_{nk}(t)$$

$$=\sum_{n=1}^{\infty}\sum_{k=1}^{\infty}D_{nk}\cos\left(\frac{n\pi}{a}x\right)\sin\left(\frac{k\pi}{L}z\right)$$

$$e^{-\frac{f}{2D}z}e^{-\left(\beta^2+\gamma^2+(\frac{f}{D}^2)\frac{1}{4}\right)Dt}, \tag{96}$$

where C_{nmk} is $A_n^*B_m^*C_k^*D_{mnk}^*$. Also, substituting Eqs. (87), (90), (95a) and (95b) into Eq. (84), the second answer for $V(x,y,z,t)$ may be written as:

$$V_2(x,y,z,t)=X_n(x)Y_1(y)Z_k^{**}(z)T_{nk}(t)$$

$$= \sum_{n=1}^{\infty}\sum_{k=1}^{\infty} D_{nk}\cos\left(\frac{n\pi}{a}x\right) \sin\left(\frac{k\pi}{L}z\right) e^{-\frac{f}{2D}z} e^{-\left(\beta^2+\gamma^2+\left(\frac{f}{D}\right)^2\frac{1}{4}\right)Dt}, \quad (97)$$

where D_{nk} is $A_n^* DC_k^{**} E_{nk}^*$. As before, Eq. (88b) also gives two answers for $V(x,y,z,t)$ as:

$$V_3(x,y,z,t) = \sum_{m=1}^{\infty}\sum_{k=1}^{\infty} A_{mk}\cos\left(\frac{m\pi}{b}y\right)\sin\left(\frac{k\pi}{L}z\right) e^{-\frac{f}{2D}z} e^{-\left(\eta^2+\gamma^2+\left(\frac{f}{D}\right)^2\frac{1}{4}\right)Dt} \quad (98)$$

$$V_4(x,y,z,t) = \sum_{k=1}^{\infty} B_k \sin\left(\frac{k\pi}{L}z\right) e^{-\frac{f}{2D}z} e^{-\left(\gamma^2+\left(\frac{f}{D}\right)^2\frac{1}{4}\right)Dt}, \quad (99)$$

where A_{mk} and B_k are constants. Also $\eta = \frac{m.\pi}{b}$, $m = 1,2,3,...,\infty$, and $\gamma = \frac{k\pi}{L}$, $k = 1,2,3,...,\infty$.

Finally, the overall answer for $V(x,y,z,t)$ is the combination of Eqs. (96) to (99):

$$\begin{aligned} V(x,y,z,t) &= V_1(x,y,z,t) + V_2(x,y,z,t) \\ &+ V_3(x,y,z,t) + V_4(x,y,z,t) \\ &= \sum_{n=1}^{\infty}\sum_{m=1}^{\infty}\sum_{k=1}^{\infty} C_{nmk}\cos\left(\frac{n\pi}{a}x\right) \cos\left(\frac{m\pi}{b}y\right)\sin\left(\frac{k\pi}{L}z\right) e^{-\frac{f}{2D}z} e^{-\left(\beta^2+\eta^2+\gamma^2+\left(\frac{f}{D}\right)^2\frac{1}{4}\right)Dt} \\ &+ \sum_{n=1}^{\infty}\sum_{k=1}^{\infty} D_{nk}\cos\left(\frac{n\pi}{a}x\right)\sin\left(\frac{k\pi}{L}z\right) e^{-\frac{f}{2D}z} e^{-\left(\beta^2+\gamma^2+\left(\frac{f}{D}\right)^2\frac{1}{4}\right)Dt} \\ &+ \sum_{m=1}^{\infty}\sum_{k=1}^{\infty} A_{mk}\cos\left(\frac{m\pi}{b}y\right)\sin\left(\frac{k\pi}{L}z\right) e^{-\frac{f}{2D}z} e^{-\left(\eta^2+\gamma^2+\left(\frac{f}{D}\right)^2\frac{1}{4}\right)Dt} \\ &+ \sum_{k=1}^{\infty} B_k \sin\left(\frac{k\pi}{L}z\right) e^{-\frac{f}{2D}z} e^{-\left(\gamma^2+\left(\frac{f}{D}\right)^2\frac{1}{4}\right)Dt}. \end{aligned} \quad (100)$$

Now, substituting Eq. (83d) into Eq. (100) and, applying Fourier series properties yields: C_{nmk}, D_{nk}, and $A_{mk} = 0$ and only B_k remains as:

$$B_k = \frac{2}{abL}\int_0^L\int_0^b\int_0^a e^{\frac{f}{2D}z}(\theta_r - P - Qe^{-\frac{f}{D}z}) \sin\left(\frac{k\pi}{L}z\right) dxdydz = \frac{2}{L}\cdot\left[(\theta_r - P)\frac{-e^{\frac{f}{2D}L}\left(\frac{k\pi}{L}\right)(-1)^k + \left(\frac{k\pi}{L}\right)}{\left(\frac{f}{2D}\right)^2 + \left(\frac{k\pi}{L}\right)^2} - Q\frac{-e^{\frac{-f}{2D}L}\left(\frac{k\pi}{L}\right)(-1)^k + \left(\frac{k\pi}{L}\right)}{\left(\frac{f}{2D}\right)^2 + \left(\frac{k\pi}{L}\right)^2}\right]. \quad (101)$$

All constant coefficients in Eq. (100) except B_k are zero. Therefore, 3D no-flow boundary infiltration problem with the initial condition of Eq. (80d) is identical to 1D infiltration problem. Substituting B_k into Eq. (100) and using Eq. (81) yields:

$$\theta(x,y,z,t) = \sum_{k=1}^{\infty} B_k \sin\left(\frac{k\pi}{L}z\right) e^{-\frac{f}{2D}z} e^{-\left(\gamma^2+\left(\frac{f}{D}\right)^2\frac{1}{4}\right)Dt} + P + Qe^{-\frac{f}{D}z}. \quad (102)$$

Eq. (102) is exactly the same as Eq. (51) derived for 2D no-flow boundary infiltration problem with initial constant water content. Water content contours for Eq. (102) at any constant y section would be similar to those depicted by Figure 12(a) and (b).

8.1. Analytical solution for 3D water infiltration with no-flow on the side boundaries and a sinusoidal initial condition

The only difference in this section (compared to the previous one) is the sinusoidal initial condition over the 3D domain, which may be mathematically expressed as:

$$\theta(x,y,z,0) = \theta_0 \sin\left(\frac{\pi x}{a}\right)\sin\left(\frac{\pi y}{b}\right)\sin\left(\frac{\pi z}{L}\right). \quad (103)$$

Substituting Eq. (103) into Eq. (83d), and then substituting the result into Eq. (100) and applying Fourier series properties give the equations shown in Box IV, where $H = \frac{f}{2D}$. Using these coefficients in Eq. (100) and substitution into Eq. (81) yields Eq. (105) as shown in Box V.

This equation is considered as the exact analytical solution to the problem since it satisfies the PDE (Eq. (57)), boundary conditions of Eq. (80a) to (80c),

and the initial condition of Eq. (103). The first four terms in Eq. (105) are functions of x, y, z, and t, reflecting unsteady behavior of the infiltrating water content front. However, the last two terms are not functions of time, and reflect the steady behavior of the front. Obviously, as $t \to \infty$, the first four terms vanish and the solution approaches that of a 1D vertical steady infiltration presented by the last two terms in Eq. (12). Problem statement dictates symmetrical water content profiles over two sections of 1) $x = a/2$ and 2) $y = b/2$; a fact that is incorporated in Eq. (105) due to the cosine terms in x and y.

Figure 16(a) to (m) depict water content contours plotted using Eq. (105) for $t = 5, 10, 15$, and 60 min, and for $y = 10, 25$, and 50 cm. The value of soil parameters used to plot these figures are identical to those used in Section 7. At early times (for all y's; Figure 16(a), (e), and (i) water content contours reflect a combination of two distinct water content gradients: 1) from center of the domain outward due to the sinusoidal initial bell shape gradient, and 2) from top to bottom (the infiltrating front) due to the gradient in water contents at top and bottom boundaries. As time elapses, the bell shape gradient attenuates, the

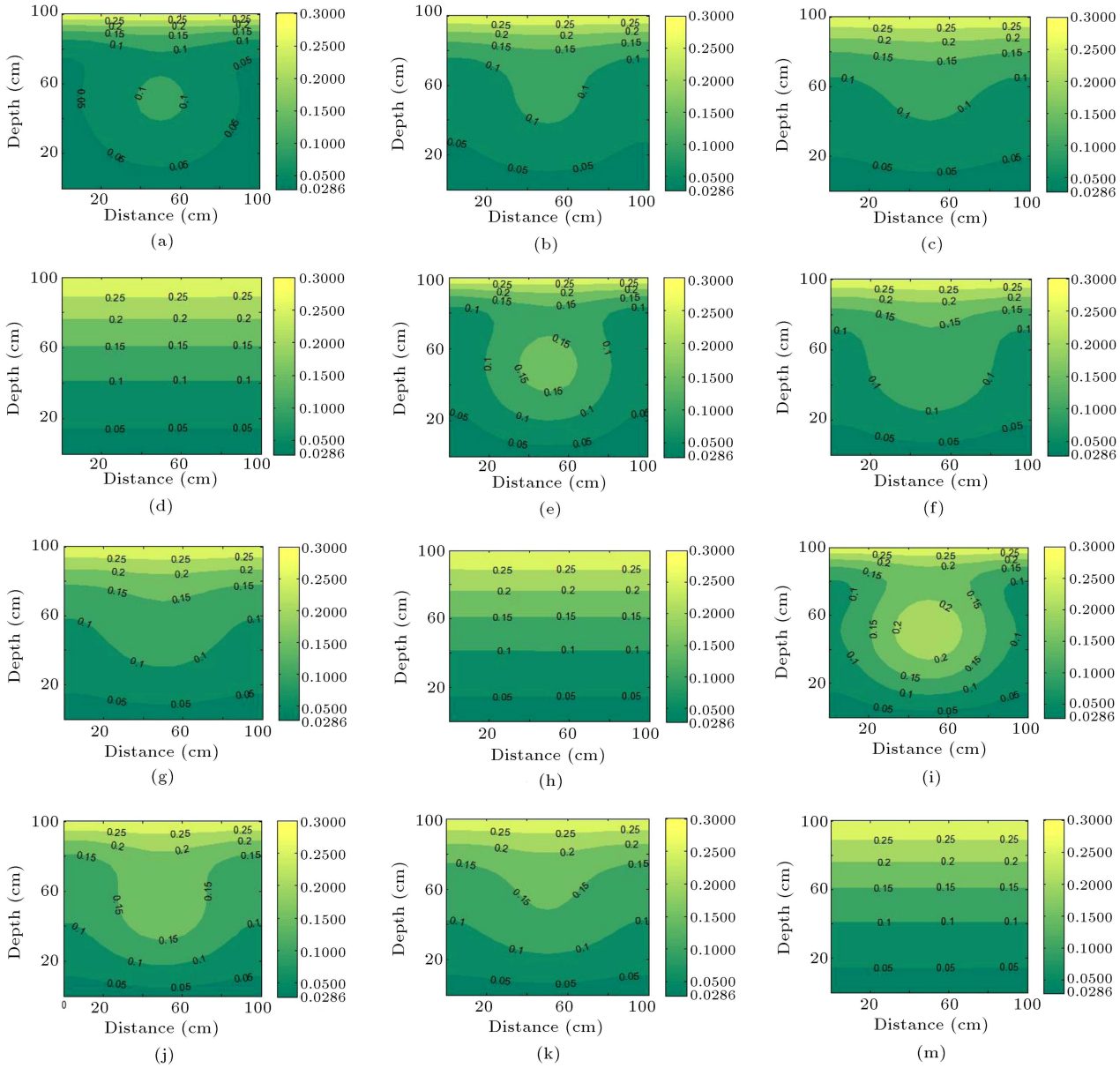

Figure 16. Water content contours plotted using Eq. (105) for (a) $y = 10$ cm and $t = 5$ min, (b) $y = 10$ cm and $t = 10$ min, (c) $y = 10$ cm and $t = 15$ min, (d) $y = 10$ cm and $t = 60$ min, (e) $y = 25$ cm and $t = 5$ min, (f) $y = 25$ cm and $t = 10$ min, (g) $y = 25$ cm and $t = 15$ min, (h) $y = 25$ cm and $t = 60$ min, (i) $y = 50$ cm and $t = 5$ min, (j) $y = 50$ cm and $t = 10$ min, (k) $y = 50$ cm and $t = 15$ min, (m) $y = 50$ cm and $t = 60$ min (other parameter values in Eq. (105) are given in the text).

$$C_{nmk} ==\frac{8}{abL}\int_0^L\int_0^b\int_0^a e^{\frac{f}{2D}z}\left(\theta_0\sin\left(\frac{\pi x}{a}\right)\sin\left(\frac{\pi y}{b}\right)\sin\left(\frac{\pi z}{L}\right)-P-Qe^{-\frac{f}{D}z}\right)\sin\left(\frac{k\pi}{L}z\right)\cos\left(\frac{n\pi}{a}x\right)$$
$$\cos\left(\frac{m\pi}{b}y\right)dxdydz$$
$$=16\theta_0\left(-\frac{HL\pi^2k\left(1+e^{HL}(-1)^k\right)}{H^4L^4+2H^2L^2\pi^2(1+k^2)+\pi^4-2\pi^4k^2+\pi^4k^4}\frac{(1+(-1)^n)}{\pi(n^2-1)}\frac{(1+(-1)^m)}{\pi(m^2-1)}\right)$$

for $n\neq 1$ and $m\neq 1$, if $n=1$ or $m=1\rightarrow C_{nmk}=0$ (104)

$$D_{nk} =\frac{4}{abL}\int_0^L\int_0^b\int_0^a e^{\frac{f}{2D}z}\left(\theta_0\sin\left(\frac{\pi x}{a}\right)\sin\left(\frac{\pi y}{b}\right)\sin\left(\frac{\pi z}{L}\right)-P-Qe^{-\frac{f}{D}z}\right)\sin\left(\frac{k\pi}{L}z\right)\cos\left(\frac{n\pi}{a}x\right)dxdydz$$
$$=8\theta_0\left(\frac{HL\pi^2k\left(1+e^{HL}(-1)^k\right)}{H^4L^4+2H^2L^2\pi^2(1+k^2)+\pi^4-2\pi^4k^2+\pi^4k^4}\frac{(1+(-1)^n)}{\pi(n^2-1)}\frac{2}{\pi}\right)$$

for $n\neq 1$ if $n=1\rightarrow D_{nk}=0$

$$A_{mk} =\frac{4}{abL}\int_0^L\int_0^b\int_0^a e^{\frac{f}{2D}z}\left(\theta_0\sin\left(\frac{\pi x}{a}\right)\sin\left(\frac{\pi y}{b}\right)\sin\left(\frac{\pi z}{L}\right)-P-Qe^{-\frac{f}{D}z}\right)\sin\left(\frac{k\pi}{L}z\right)\cos\left(\frac{m\pi}{b}y\right)dxdydz$$
$$=8\theta_0\left(\frac{HL\pi^2k\left(1+e^{HL}(-1)^k\right)}{H^4L^4+2H^2L^2\pi^2(1+k^2)+\pi^4-2\pi^4k^2+\pi^4k^4}\frac{(1+(-1)^m)}{\pi(m^2-1)}\frac{2}{\pi}\right)$$

for $m\neq 1$ if $m=1\rightarrow A_{mk}=0$

$$B_k=\frac{2}{abL}\int_0^L\int_0^b\int_0^a e^{\frac{f}{2D}z}\left(\theta_0\sin\left(\frac{\pi x}{a}\right)\sin\left(\frac{\pi y}{b}\right)\sin\left(\frac{\pi z}{L}\right)-P-Qe^{-\frac{f}{D}z}\right)\sin\left(\frac{k\pi}{L}z\right)dxdydz$$
$$=\frac{2}{abL}\left(\frac{-2HL\pi^2k\left(1+e^{HL}(-1)^k\right)\theta_0}{H^4L^4+2H^2L^2\pi^2(1+k^2)+\pi^4-2\pi^4k^2+\pi^4k^4}\frac{4}{\pi^2}+P\frac{k\pi\left(-1+e^{HL}(-1)^k\right)}{H^2L^2+k^2\pi^2}\right.$$
$$\left.-Q\frac{k\pi\left(e^{Hl}-(-1)^k\right)e^{-HL}}{H^2L^2+k^2\pi^2}\right)$$

Box IV

1D vertical infiltration prevails (Figure 16(d), (h), and (m), and eventually water content contours approach a steady state exponential profile associated with the last two terms in Eq. (105).

Figure 17(a) and (b) show 3D plots of water content contours at $y=50$ cm section (middle section of the cubic domain) for $t=5$ and 10 min. These figures are actually 3D plots of Figure 16(i) and (j), respectively. Comparison of Figure 17(a) and (b) shows how the initial condition of a "water content hump" in the middle of the cube, and boundary conditions of a sharp water content gradient interact, as the time elapses. As shown, the peak of the "hump" attenuates while water content near the side boundaries increase and their combination approach the final steady state water content distribution over the domain.

9. Conclusions

New analytical solutions to Richards' equation in one, two, and three dimensions subject to various boundary and initial conditions were presented using separation of variables and Fourier series expansion techniques. Solutions have the general form of infinite series with exponential terms whereby both steady and unsteady solutions may be obtained from a single closed form so-

$$\theta(x,y,z,t) = \sum_{n=1}^{\infty}\sum_{m=1}^{\infty}\sum_{k=1}^{\infty} C_{nmk}\cos\left(\frac{n\pi}{a}x\right)\cos\left(\frac{m\pi}{b}y\right)\sin\left(\frac{k\pi}{L}z\right)e^{-\frac{f}{2D}z}e^{-\left(\beta^2+\eta^2+\gamma^2+\left(\frac{f}{D}\right)^2\frac{1}{4}\right)Dt}$$
$$+\sum_{n=1}^{\infty}\sum_{k=1}^{\infty} D_{nk}\cos\left(\frac{n\pi}{a}x\right)\sin\left(\frac{k\pi}{L}z\right)e^{-\frac{f}{2D}z}e^{-\left(\beta^2+\gamma^2+\left(\frac{f}{D}\right)^2\frac{1}{4}\right)Dt}$$
$$+\sum_{m=1}^{\infty}\sum_{k=1}^{\infty} A_{mk}\cos\left(\frac{m\pi}{b}y\right)\sin\left(\frac{k\pi}{L}z\right)e^{-\frac{f}{2D}z}e^{-\left(\eta^2+\gamma^2+\left(\frac{f}{D}\right)^2\frac{1}{4}\right)Dt}+\sum_{k=1}^{\infty} B_k$$
$$\sin\left(\frac{k\pi}{L}z\right)e^{-\frac{f}{2D}z}e^{-\left(\gamma^2+\left(\frac{f}{D}\right)^2\frac{1}{4}\right)Dt}+Qe^{-\frac{f}{D}z}+P \qquad (105)$$

Box V

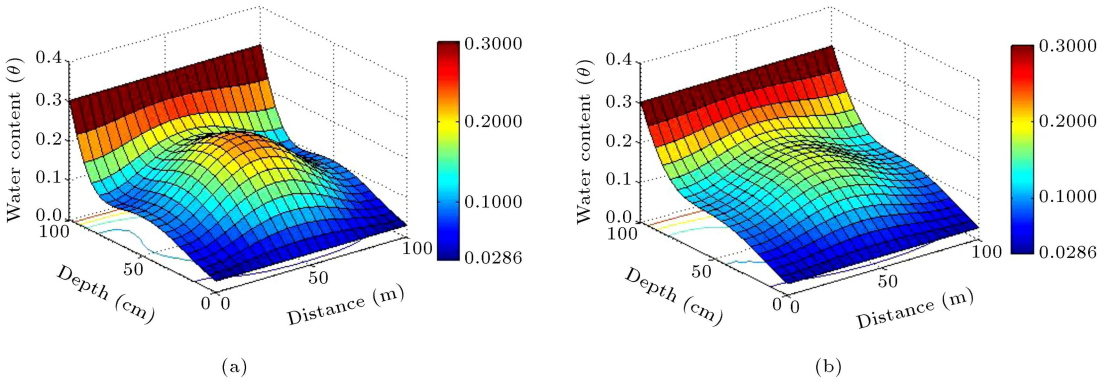

Figure 17. 3D plots of Eq. (105) for $y = 50$ cm: (a) $t = 5$ min and (b) $t = 10$ min (other parameter values in Eq. (105) are given in the text).

lution. Analytical solutions for 1 and 2D horizontal and vertical water infiltration were compared to numerical finite difference method solutions and shown to have less than 2% difference. Solutions to 2 and 3D vertical water infiltration were derived for constant, no-flow, and sinusoidal boundary and initial conditions. The solutions may be utilized to test numerical models that use different computational techniques.

References

1. Bear, J. and Chang, A.H., *Modeling Groundwater Flow and Contaminant Transport*, Springer Interscience Publication (2010).
2. An, H., Ichikawa, Y., Tachikawa, Y. and Shiiba, M. "A new iterative alternating direction implicit (IADI) algorithm for multi-dimensional saturated-unsaturated flow", *Journal of Hydrology*, **408**, pp. 127-139 (2011).
3. An, H., Ichikawa, Y., Tachikawa, Y. and Shiiba, M. "Comparison between iteration schemes for three-dimensional coordinate-transformed saturated-unsaturated flow model", *Journal of Hydrology*, **470-471**, pp. 212-226 (2012).
4. Diaw, E.B., Lehmann, F. and Ackerer, P. "One dimensional simulation of solute transfer in saturated-unsaturated porous media using the discontinuous finite elements method", *Journal of Contaminant Hydrology*, **51**, pp. 197-213 (2001).
5. Manzini, G. and Ferraris, S. "Mass-conservative finite volume methods on 2D unstructured grids for the Richards equation", *Advances in Water Resources*, **27**, pp. 1199-1215 (2004).
6. Solin, P. and Kuraz, M. "Solving the nonstationary Richards equation with adaptive hp-FEM", *Advances in Water Resources*, **34**, pp. 1062-1081 (2011).
7. Paulus, R., Dewals, B.J., Erpicum, S., Pirotton, M. and Archambeau, P. "Innovative modelling of 3D unsaturated flow in porous media by coupling independent models for vertical and lateral flows", *Journal of Computational and Applied Mathematics*, **246**, pp. 38-51 (2013).
8. Fahs, M., Younes, A. and Lehmann, F. "An easy and efficient combination of the mixed finite element method and the method of lines for the resolution of Richards' Equation", *Environmental Modelling & Software*, **24**, pp. 1122-1126 (2009).
9. Montazeri Namin, M. and Boroomand, M.R. "A time splitting algorithm for numerical solution of Richard's

equation", *Journal of Hydrology*, **444-445**, pp. 10-21 (2012).

10. Johari, A. and Hooshmand, N. "Prediction of soil-water characteristic curve using Gene expression programming", *Iranian Journal of Science & Technology, Transactions of Civil Engineering*, **39**(C1), pp. 143-165 (2015).
11. Akbari, A., Ardestani, M. and Shayegan, J. "Distribution and mobility of petroleum hydrocarbons in soil: case study of the South Pars gas complex, Southern Iran", *Iranian Journal of Science & Technology, Transactions of Civil Engineering*, **36**(C2), pp. 265-275 (2012).
12. Parlange, J.Y., Barry, D.A., Parlange, M.B., Hogarth, W.L., Haverkamp, R., Ross, P.J., Ling, L. and Steenhuis, T.S. "New approximate analytical technique to solve Richards equation for arbitrary surface boundary conditions", *Water Resources Research*, **33**(4), pp. 903-906 (1997).
13. Mollerup, M. "Philip's infiltration equation for variable-head ponded infiltration", *Journal of Hydrology*, **347**, pp. 173-176 (2007).
14. Menziani, M., Pugnaghi, S. and Vincenzi, S. "Analytical solutions of the linearized Richards equation for discrete arbitrary initial and boundary conditions", *Journal of Hydrology*, **332**, pp. 214-225 (2007).
15. Tracy, F.T. "Clean two- and three-dimensional analytical solutions of Richards'equation for testing numerical solvers", *Water Resources Research*, **42**(8), W08503 (2006).
16. Tracy, F.T. "Three-dimensional analytical solutions of Richards' equation for a box-shaped soil sample with piecewise-constant head boundary conditions on the top", *Journal of Hydrology*, **336**, pp. 391-400 (2007).
17. Wang, Q.J., Horton, R. and Fan, J. "An analytical solution for one-dimensional water infiltration and redistribution in unsaturated soil", *Pedosphere*, **19**(1), pp. 104-110 (2009).
18. Ghotbi, A.R., Omidvar, M. and Barari, A. "Infiltration in unsaturated soils - An analytical approach", *Computers and Geotechnics*, **38**, pp. 777-782 (2011).
19. Nasseri, M., Daneshbod, Y., Pirouz, M.D., Rakhshandehroo, G.R. and Shirzad, A. "New analytical solution to water content simulation in porous media", *Journal of Irrigation and Drainage Engineering*, **138**, pp. 328-335 (2012).
20. Brooks, R.H. and Corey, A.T., *Hydraulic Properties of Porous Media*, Colorado State University, Fort Collins, CO., Hydrology Paper No. 3 (1964).
21. Huang, R.Q. and Wu, L.Z. "Analytical solutions to 1-D horizontal and vertical water infiltration in saturated/unsaturated soils considering time-varying rainfall", *Computers and Geotechnics*, **39**, pp. 66-72 (2012).
22. Asgari, A., Bagheripour, M.H. and Mollazadeh, M. "A generalized analytical solution for a nonlinear infiltration equation using the exp-function method", *Scientia Iranica*, **18**(1), pp. 28-35 (2011).
23. Basha, H.A. "Infiltration models for soil profiles bounded by a water table", *Water Resource Research*, **47**, W10527 (2011).
24. He, J.H. "Approximate analytical solution for seepage flow with fractional derivatives in porous media", *Computer Methods in Applied Mechanics and Engineering*, **167**(1-2), pp. 57-68 (1998).
25. Moghimi, M. and Hejazi, F. "Variational iteration method for solving generalized Burger-Fisher and Burger equations", *Chaos Solitons and Fractals*, **33**, pp. 1756-1761 (2007).
26. Wazwaz, A.M. "A comparison between the variational iteration method and Adomian decomposition method", *Journal of Computational and Applied Mathematics*, **207**(1), pp. 129-136 (2007).
27. Nasseri, M., Shaghaghian, M.R., Daneshbod, Y. and Seyyedian, H. "An analytic solution of water transport in unsaturated porous media", *Journal of Porous Media*, **11**(6), pp. 591-601 (2008).
28. Serrano, S.E. and Adomian, G. "New contribution to the solution of transport equation in porous media", *Mathematical Computational Modelling*, **24**, pp. 15-25 (1996).
29. Serrano, S.E. "Analytical decomposition of the nonlinear unsaturated flow equation", *Water Resource Research*, **31**, pp. 2733-2742 (1998).
30. Serrano, S.E. "Modeling infiltration with approximate solutions to Richards' equation", *Journal of Hydraulic Engineering*, **9**, pp. 421-432 (2004).
31. Pamuk, S. "Solution of the porous media equation by Adomian's decomposition method", *Physics Letters*, **344**, pp. 184-188 (2005).
32. Zlotnik, V.A., Wang, T., Nieber, J.L. and Simunek, J. "Verification of numerical solutions of the Richards equation using a traveling wave solution", *Advance Water Resource*, **30**, pp. 1973-1980 (2007).
33. Basha, H.A. "Multidimensional linearized nonsteady infiltration with prescribed boundary conditions at the soil surface", *Water Resource Research*, **35**(1), pp. 75-83 (1999).
34. Carr, E.J., Moroney, T.J. and Turner, I.W. "Efficient simulation of unsaturated flow using exponential time integration", *Applied Mathematics and Computation*, **217**, pp. 6587-6596 (2011).
35. Jaiswal, D.K., Kumar, A. and Yadav, R.R. "Analytical solution to the one-dimensional advection-diffusion equation with temporally dependent coefficients", *Water Resource*, **3**, pp. 76-84 (2011).
36. Richards, L.A. "Capillary conduction of liquids through porous mediums", *Physics*, **1**, pp. 318-333 (1931).
37. Van Genuchten, M.T. "A closed-form equation for predicting the hydraulic conductivity of unsaturated soils", *Soil Science Society of America Journal*, **44**(5), pp. 892-898 (1980).

38. Haverkamp, R., Parlange, J.Y., Starr, J.L., Schmiz, G.H. and Fuentes, C. "Infiltration under ponded conditions: A predictive equation based on physical parameters", *Soil Science Journal*, **149**(5), pp. 292-300 (1990).

39. Fredlund, D.G. and Xing, A. "Equations for soil-water characteristic curve", *Canadian Geotechnical Journal*, **31**(4), pp. 521-532 (1994).

Biographies

Hamed Reza Zarif Sanayei is PhD student at the Department of Civil and Environmental Engineering at Shiraz University, Shiraz, Iran. He holds BS degree of Shahid Chamran University in Civil Engineering and MS degree of Shiraz University in Hydraulic Structures.

Gholam Reza Rakhshandehroo is currently a Professor of Civil and Environmental Engineering at Shiraz University. He has published many ISI papers. He is actively involved in teaching, research and consulting works in areas of groundwater (saturated and unsaturated zones) water research, hydraulic engineering.

Nasser Talebbeydokhti is currently a Professor of Civil and Environmental Engineering at Shiraz University. He is the Editor-in-Chief of the Iranian Journal of Science and Technology Transactions of Civil Engineering. Also, Professor Talebbeydokhti is a member of Academy of Sciences of Iran. He has published many ISI papers. He is actively involved in teaching, research and consulting works in areas of water research, hydraulic structures and environmental engineering.